

Optical properties of atmospheric fine particles near Beijing during the HOPE-J³A Campaign

X. Xu^{1,2,3}, W. Zhao^{1,2}, Q. Zhang^{1,2,3}, S. Wang^{1,2,3}, B. Fang^{1,2}, W. Chen⁵, D. S. Venables^{6,7}, X. Wang⁸,
W. Pu⁹, X. Wang⁹, X. Gao^{1,2,4}, and W. Zhang^{1,2,4}

¹ Key Laboratory of Atmospheric Composition and Optical Radiation, Anhui Institute of Optics and Fine Mechanics, Chinese Academy of Sciences, Hefei 230031, Anhui, China

² Laboratory of Atmospheric Physico-Chemistry, Anhui Institute of Optics and Fine Mechanics, Chinese Academy of Sciences, Hefei, 230031, Anhui, China

³ Graduate School, University of Science and Technology of China, Hefei, 230026, Anhui, China

⁴ School of Environmental Science and Optoelectronic Technology, University of Science and Technology of China, Hefei, 230026, Anhui, China

⁵ Laboratoire de Physicochimie de l'Atmosphère, Université du Littoral Côte d'Opale, 59140 Dunkerque, France

⁶ Department of Chemistry and Environmental Research Institute, University College Cork, Cork, Ireland

⁷ Leibniz Institute for Tropospheric Research, 04318 Leipzig, Germany

⁸ Environment Research Institute, Shandong University, Jinan 250100, China

⁹ Key Laboratory for Semi-Arid Climate Change of the Ministry of Education, College of Atmospheric Sciences, Lanzhou University, Lanzhou 730000, China

*Correspondence to :

W. Zhao (wxzhao@aiofm.ac.cn) and W. Zhang (wjzhang@aiofm.ac.cn)

1 **Abstract**

2 The optical properties and chemical composition of PM_{1.0} particles in a suburban environment
3 (Huairou) near the mega-city of Beijing were measured during the HOPE-J³A (Haze Observation
4 Project Especially for Jing-Jin-Ji Area) field campaign. The campaign covered the period November
5 2014 to January 2015 during the winter coal heating season. The average values and standard
6 deviations of the extinction, scattering, absorption coefficients, and the aerosol single scattering
7 albedo (SSA) at $\lambda = 470$ nm during the measurement period were 201 ± 240 , 164 ± 202 , 37 ± 43
8 Mm^{-1} , and 0.80 ± 0.08 , respectively. The mean mass scattering (MSE) and absorption (MAE)
9 efficiencies of PM_{1.0} were 3.6 and 0.7 $\text{m}^2 \text{g}^{-1}$, respectively. Highly time-resolved air pollution
10 episodes clearly show the dramatic evolution of the PM_{1.0} size distribution, extensive optical
11 properties (extinction, scattering, and absorption coefficients) and intensive optical properties (single
12 scattering albedo and the effective complex refractive index, CRI) during haze formation,
13 development and decline. Time periods were classified into three different pollution levels (clear,
14 slightly polluted, and polluted) for further analysis. It was found that: (1) The diurnal patterns of the
15 aerosol extinction, scattering, absorption coefficients, and SSA differed for the three pollution classes.
16 (2) The real and imaginary part of the effective CRI increased, while the SSA decreased from clear
17 to polluted days. (3) The relative contributions of organic and inorganic species to observed aerosol
18 composition changed significantly from clear to polluted days: the organic mass fraction decreased
19 from 50% to 43% while the proportion of sulfates, nitrates, and ammonium increased strongly from
20 34% to 44%. (4) The fractional contribution of chemical components to extinction coefficients was
21 calculated by using the modified IMPROVE algorithm. Organic mass was the largest contributor
22 (58%) to the total extinction of PM_{1.0}. When the air quality deteriorated, the change of the relative
23 contribution of sulfate aerosol to the total extinction was small, but the contribution of nitrate aerosol
24 increased significantly (from 17% on clear days to 23% on polluted days). (5) The observed mass
25 scattering efficiencies of PM_{1.0} increased with the extent of pollution, whereas the observed mass
26 absorption efficiencies of PM_{1.0} increased in slightly polluted conditions but decreased under
27 polluted conditions.

28

29

30

1 **1 Introduction**

2

3 Atmospheric aerosols have significant effects on climate forcing (Ramanathan et al., 2001;
4 Anderson et al., 2003; Wang et al., 2010; Bahadur et al., 2012), environment (Cao et al., 2013;
5 Huang et al., 2014), and human health (Nel, 2005; S. Zheng et al., 2015). Visibility is regarded as an
6 indicator of air quality and is affected by the scattering and absorption of solar light by fine particles
7 (Watson, 2002). Uncertainties in atmospheric visibility are mainly due to the uncertainties associated
8 with the aerosols' optical properties, which depend on the physical and chemical properties of
9 atmospheric aerosol, including chemical composition, size distribution, mixing state, morphology
10 and hygroscopic properties. Understanding how these physical and chemical characteristics affect the
11 optical properties of particles is key to improve quantitative estimates of direct radiative forcing and
12 to determine the environmental effects of particles. To ascertain the relationships between these
13 parameters, many research campaigns have been performed during the past decade, including ACE-1
14 (Bates et al., 1998), ACE-2 (Raes et al., 2000), INDOEX (Eldering, 2002), ACE-Asia (Quinn, 2004;
15 Doherty et al., 2005), PRIDE-PRD2004 (Zhang et al., 2008), MILAGRO (Marley et al., 2009),
16 CAREBeijing (Jung et al., 2009; Garland et al., 2009; Wu et al., 2011) and CalNex campaign (Cahill
17 et al., 2012; Thompson et al., 2012; Ryerson et al., 2013; X. Zhang et al., 2013).

18 Rapid urbanization and economic development has brought about serious environmental
19 problems in the megacities of China (L. Han et al., 2015). The North China Plain (NCP) region in
20 northeast China has one of the highest global aerosol concentrations (Sun et al., 2013) due to the
21 dense population, the large number of vehicles, and intense industrial activity. The China National
22 Ambient Air Quality Standard designates a daily average concentration of $PM_{2.5}$ greater than $75 \mu g$
23 m^{-3} as harmful to health. However, $PM_{2.5}$ concentrations in China often grossly exceed this limit –
24 for instance, daily average mass concentration of $PM_{2.5}$ in January 2013 were higher than $500 \mu g m^{-3}$
25 for Beijing (Andersson et al., 2015). A large amount of atmospheric pollutants are emitted from
26 fossil fuel, biomass burning and urban construction (Lei et al., 2011; Zhang et al., 2011). The
27 mixture of these various emissions results in complex physical, chemical and optical properties of
28 aerosols in the NCP region.

29 In recent years, many campaigns have been conducted in Beijing to study the relationships
30 between the mass concentrations, optical properties, chemical components, hygroscopic properties,

1 mixing state, new particle formation, light apportionment and meteorological conditions (Liu et al.,
2 2013; Sun et al., 2013, 2015; Guo et al., 2014; Andersson et al., 2015; B. Han et al., 2015; Wang et
3 al., 2015; Wu et al., 2015; Xu et al., 2011; X. J. Zhao et al., 2013; G. J. Zheng et al., 2015). It is
4 worth noting that atmospheric dynamic processes differ between polluted and cleaner periods and
5 that secondary aerosols have been proposed as the major contributor to haze formation (Quan et al.,
6 2014; Y. L. Sun et al., 2014). Research in the Pearl River Delta of China has shown that submicron
7 particles contribute more than 90% of the particle extinction (Cheng et al., 2008). However, few
8 studies in the NCP region have focused on light extinction contribution of submicron aerosol under
9 different air pollution conditions. Moreover, the evolution of intensive optical properties (effective
10 complex refractive index, CRI, and single scattering albedo, SSA, ω , the ratio of scattering to
11 extinction) in haze formation, development and decline have rarely been reported. Comprehensive
12 studies of intensive optical properties and light apportionment are necessary for a better
13 understanding of the evolution of aerosol physical and optical properties in the NCP.

14 In this paper, we report continuous measurements of the optical properties, particle size
15 distributions, and chemical composition of submicron aerosol at a suburban site (Huairou) from 16
16 November 2014 to 11 January 2015. The effective CRI for $PM_{1.0}$ particles were retrieved with Mie
17 theory by treating the submicron aerosols as spherical particles. The fractional contribution of the
18 chemical components of particles to the total extinction coefficient were calculated by the modified
19 IMPROVE algorithm (Pitchford et al., 2007). $PM_{1.0}$ optical properties, chemical compositions, size
20 distributions, chemical apportionment of light extinction, and mass scattering and absorption
21 efficiencies are reported for three different pollution levels (clear, slight polluted, and polluted days).
22 The results show that there was a large amount of light absorbing fine particles in Beijing in the
23 winter time over the campaign period.

24 25 **2 Experimental**

26
27 The Haze Observation Project Especially for Jing-Jin-Ji (Beijing-Tianjin-Hebei, the national
28 capital region of China) Area (HOPE-J³A) field campaign took place at the Huairou campus of the
29 University of Chinese Academy of Sciences (40°24'24.45"N, 116°40'32.95"E) from October 2014 to
30 January 2015. The goal of the HOPE-J³A campaign was to better understand the emissions, transport,

1 and evolution of atmospheric fine particles and their precursors in the Jing-Jin-Ji area. Figure 1
2 shows the map of NCP and the average distribution of the MODIS (MODerate-resolution Imaging
3 Spectroradiometer) (Chu et al., 2003) AOD (aerosol optical depth) with a resolution of $0.2^\circ \times 0.2^\circ$
4 during the field campaign from 16 November 2014 to 11 January 2015. The Huairou observation site
5 (marked as a red star in Fig. 1) is situated about 60 km northeast of Beijing city center and is mainly
6 surrounded by medium density residential suburban areas.

7 The instruments were installed on the 4th floor of Teaching Building 1, with the sample inlet
8 about 2.5 m above the roof. The inlet consisted of a $PM_{1.0}$ ambient size cut (SF- $PM_{1.0}$, $1.0 \text{ m}^3 \text{ h}^{-1}$,
9 Sven Leckel Ingenieurburo GmbH) with a 50% cut-point at $1.0 \mu\text{m}$. Downstream of the inlet, the
10 sample air was dried to below 15% RH by a diffusion dryer and then passed through a copper tube (6
11 m long with an inner diameter of 1 cm) at a flow rate of 38 L min^{-1} .

12 The particle size distribution between 14 and 662 nm was measured every 3 min with a scanning
13 mobility particle sizer (SMPS, TSI 3936), which comprised an electrostatic classifier (TSI 3080) and
14 a condensation particle counter (TSI 3776). Diffusion losses and the effect of multicharged particles
15 were corrected by the instrument software. The SMPS was validated with laboratory-generated,
16 NIST traceable monodispersed polystyrene latex (PSL) spheres with diameters of $203 \pm 5 \text{ nm}$
17 (Thermo Scientific 3200A) and $296 \pm 6 \text{ nm}$ (Thermo Scientific 3300A) before and after the
18 campaign (W. Zhao et al., 2013). The measured particle sizes and the certified diameters of the PSL
19 spheres agreed to within 2 %.

20 The optical properties of $PM_{1.0}$ particles were measured with a newly developed cavity-enhanced
21 albedometer (Zhao et al., 2014a). The albedometer was based on a blue light-emitting-diode (LED)
22 incoherent broadband cavity-enhanced absorption spectroscopy (IBBCEAS) system that
23 incorporated an integrating sphere (IS). This instrument is a new tool for direct, in situ, and
24 simultaneous measurement of aerosol scattering and extinction coefficients (and thus of the
25 absorption coefficient and aerosol SSA, ω_{470}) at a mean wavelength of 470 nm. The performance of
26 the cavity-enhanced albedometer was previously evaluated using laboratory-generated, monodisperse
27 standard aerosol particles, and the scattering measurements were also found to be in close agreement
28 with TSI 3563 nephelometer measurements (Zhao et al., 2014 a, b).

29 The advantage of broadband over single wavelength measurements is its capacity to
30 simultaneously measure multiple species present in the sample (gases and particles) using a single

1 instrument. A spectral-fitting algorithm was applied from 445 to 480 nm to retrieve gas
2 concentrations based on their spectral structure and thereby to remove the contribution of gas phase
3 absorption from the aerosol extinction. The scattering signal in the IS was measured by a single
4 channel photomultiplier tube (PMT), providing an integrated result over a narrow bandwidth of ~ 9
5 nm (full-width at half maximum, FWHM) in the spectral region of 465–474 nm. Truncation
6 reduction tubes (Varma et al., 2003) were used to minimize the forward and backward truncation
7 angles to 1.2°.

8 The sample volume of the system was about 1.8 L and the flow rate of the cavity-enhanced
9 albedometer was 1.5 L min⁻¹ at atmospheric pressure. The acquisition time for each measurement
10 was 9 s (for a 1.5 s integrating time per spectrum, and six-spectra averaging). The temperature and
11 relative humidity of the sample were measured with a hygrometer (Rotronic, model HC2 humidity
12 sensor). The cavity was flushed with dry zero air every hour to acquire a reference spectrum. The
13 reference spectrum was used both in the IBBCEAS retrieval (Fiedler et al., 2003) and to remove the
14 contribution of light scattering from internal surfaces and Rayleigh scattering. The mirror reflectivity
15 $R(\lambda)$ and the scaling factor (K' , the calibration coefficient that related instrument response to
16 scattering magnitude) for the scattering channel of the albedometer were determined by He, N₂ and
17 CO₂ every week. No deterioration of R and K' were observed during the campaign.

18 The detection limits for the scattering and extinction channels with 9 s integration time were
19 0.54 Mm⁻¹ and 0.15 Mm⁻¹, respectively. The total uncertainty in the extinction measurement was
20 estimated to be less than 4% and arose from uncertainties in the mirror reflectivity (R) (~1%), the
21 ratio of cavity length to the cell length containing the air sample when the cavity mirrors were purged
22 (R_L) (~3%), and particle losses in the system (~2%). The total uncertainty in the scattering
23 measurement was about 3%, with dominant contributions from uncertainties in the experimentally
24 determined scattering calibration coefficient (K') (2%), and the uncertainty associated with particle
25 losses in the cavity (2%).

26 Based on a Mie scattering calculation, the truncated fraction of total scattering was about 0.22%
27 for a 1 μm diameter spherical particle with a complex refractive index (CRI) of $m = 1.6 + i0$ at $\lambda =$
28 470 nm. This truncation effect was therefore negligible compared to the measurement uncertainty
29 and no correction for the truncation underestimate was applied to our data.

30 Potential uncertainties associated with changes in the instrument environment were considered

1 but found to be unimportant. The instrument was located in a temperature-controlled room, the
2 temperature inside the albedometer enclosure was maintained at $28.3 \pm 0.8^\circ\text{C}$, and the sample flow
3 was controlled with a mass flow meter. Example data of the transmitted intensity measured with the
4 CCD spectrometer and the scattering signal measured with the PMT are shown in Fig. S1 in the
5 supplement. The cavity was flushed with particle-free air every hour to acquire the $I_0(\lambda)$ spectrum.
6 No obvious drift in the LED light intensity was observed even after 6 hours of measurement,
7 indicating the high stability of the instrument under these operating conditions.

8 Another $\text{PM}_{1.0}$ sampler (SF- $\text{PM}_{1.0}$, Sven Leckel Ingenieurburo GmbH) was installed on the roof
9 of the building ($\sim 20\text{m}$ above the ground) to collect $\text{PM}_{1.0}$ samples with quartz filters (47 mm,
10 MUNKTELL Corporation) for off-line aerosol chemical composition analysis. The flow rate was 38
11 L min^{-1} and samples were collected over the period of 16 November 2014 to 11 January 2015. The
12 collection time period was 12 h: from 08:30 to 20:30 LT for daytime samples, and from 20:30 to
13 08:30 LT for nighttime samples. Before sampling, the quartz-fiber filters were preheated for 4 h at
14 600°C in a muffle furnace, and ten filters were used as field blank samples in the sampling period. In
15 total, 114 filters were collected; these were stored at -4°C to prevent evaporation of volatilized
16 species until they were analyzed.

17 A punch of 1.5 cm^2 was taken from each filter, and then heated in inert and oxidizing
18 atmospheres to volatilize and combust the loaded carbon, respectively. The carbon (elemental carbon,
19 EC, and organic carbon, OC) concentrations were determined with a thermal/optical transmittance
20 aerosol carbon analyzer (Sunset Laboratory, Inc.) (NIOSH, 1996). The measurement principle and
21 operation of the Sunset aerosol carbon analyzer was presented in a previous study (Peterson et al.,
22 2002). Another punch with a area of 2 cm^2 was taken from the rest of filter, extracted into 10 mL of
23 deionized water ($> 18\text{M}\Omega$) via 20 min sonication, filtered using a $0.22 \mu\text{m}$ PTFE syringe filter, and
24 stored in a refrigerator at 4°C until chemical analysis. Eight water-soluble ion compositions [three
25 anions: nitrate (NO_3^-), sulfate (SO_4^{2-}), and chloride (Cl^-); five cations: ammonium (NH_4^+), sodium
26 (Na^+), potassium (K^+), magnesium (Mg^{2+}) and calcium (Ca^{2+})] were determined using a Dionex
27 ICS-90 Ion Chromatography system with AS14A and CS14A columns and eluents of
28 $\text{NaCO}_3\text{-NaHCO}_3$ and methanesulfonic acid, respectively. Further details on this analysis are given
29 elsewhere (X. F. Wang et al., 2013).

30 Meteorological parameters, including wind speed (WS) and direction (WD), temperature (T) and

1 relative humidity (RH), were continuously recorded at the observation site. The mass concentration
 2 of PM_{2.5} for the air quality classification and concentrations of pollutant gases (SO₂, NO₂, O₃, and
 3 CO) were monitored by the National Environmental Bureau and the data at Huairou were retrieved
 4 from the internet (<http://113.108.142.147:20035/emcpublish/>). In this work, the PM_{2.5} pollution level
 5 was divided into three categories according to the technical regulation on Ambient Air Quality Index
 6 (National Environmental Protection Standard of the People's Republic of China, HJ 633–2012)
 7 (http://kjs.mep.gov.cn/hjbhbz/bzwb/dqhjbh/jcg_fbz/201203/W020120410332725219541.pdf; A.
 8 Zhang et al., 2013; G. J. Zheng et al., 2015): clear day (PM_{2.5} concentration ≤ 35 μg m⁻³, when the
 9 corresponding individual air quality index (IAQI) of 24 hours averaged PM_{2.5} concentration ranged
 10 from 0 to 50), slightly polluted day (35 μg m⁻³ < PM_{2.5} concentration ≤ 115 μg m⁻³, when IAQI of
 11 PM_{2.5} ranged from 50 to 150), and polluted day (115 μg m⁻³ < PM_{2.5} concentration ≤ 350 μg m⁻³,
 12 when IAQI of PM_{2.5} ranged from 150 to 400). These pollution classes are usually based on PM_{2.5}
 13 concentrations averaged from 00:00 to 23:59 on a specific date. For our filter samples, however, the
 14 collection time extended over two days; nevertheless, we applied the same categorization for our
 15 measurements from 20:30 (day 1) to 20:30 LT (day 2).

17 3 Optical data analysis method

19 3.1 Retrieval of aerosol complex refractive index

21 The scattering and extinction coefficients of particles are calculated based on (Pettersson et al.,
 22 2004):

$$23 \alpha_{ep,sp} = \int N(D_p) \frac{\pi}{4} D_p^2 Q_{ext,scat}(m, x) dD_p \quad (1)$$

24 where $x = \pi D_p / \lambda$ is the size parameter, $m = n + i k$ is the CRI of the particle (where n and k
 25 correspond to the real and imaginary parts of the CRI, respectively), N is the number of particles per
 26 unit volume in the size bin dD_p with mean diameter D_p , and $\frac{\pi}{4} D_p^2 Q_{ext,scat}(m, x)$ is the extinction or
 27 scattering cross section $\sigma_{ep,sp}$. The extinction or scattering efficiency, $Q_{ext,scat}$, is a function of the CRI,
 28 the morphology of the particles and the size parameter. For chemically homogeneous spherical

1 particles, Q can be calculated from Mie theory.

2 The effective CRI is an effective property that averages over the aerosols' size, shape, mixing
3 state and chemical composition. Simultaneous measurement of the scattering and extinction
4 coefficients by the cavity-enhanced albedometer provides a new approach for faster retrieval of the
5 particulate CRI (Riziq et al., 2007; Mack et al., 2010; Zhao et al., 2014a; Xu et al., 2016). Details of
6 the CRI retrieval have been given in previous studies (Riziq et al., 2007; Mack et al., 2010). The
7 measured extinction and scattering coefficients ($\alpha_{ep,470}$ and $\alpha_{sp,470}$) and the particle number size
8 distribution, $N(D_p)$, were used to determine the effective CRI on the assumption that particles were
9 spherical and that the black carbon aerosol (BC) can be treated in a volume mixing approach. The
10 real and imaginary parts of the effective CRI were varied (between 1.3 and 1.7 for the real part and
11 between 0 and 0.1 for the imaginary part) to calculate the extinction and scattering coefficients for
12 each size distribution. A set of refractive indices were determined by finding the minimum of the
13 “merit function”, χ^2 (Mack et al., 2010):

$$\chi^2 = \frac{(\alpha_{ep} - \alpha_{ep_calc})^2}{\varepsilon_{\alpha_{ep}}^2} + \frac{(\alpha_{sp} - \alpha_{sp_calc})^2}{\varepsilon_{\alpha_{sp}}^2} \quad (2)$$

15 Here, α_{ep} and α_{sp} are the measured values of the extinction and scattering coefficients, while α_{ep_calc}
16 and α_{sp_calc} are the corresponding calculated values. $\varepsilon_{\alpha_{ep}}$ and $\varepsilon_{\alpha_{sp}}$ are the measurement uncertainty of
17 α_{ep} and α_{sp} , respectively. The mean standard deviations of the extinction and scattering coefficients
18 over 3 min were taken as the measurement uncertainty for calculating χ^2 .

19 A contour plot of χ^2 versus n and k was used to estimate the standard errors of n and k . The
20 values of n and k that satisfied $\chi^2 < \chi_0^2 + 2.298$, which fell within the 1σ error bound of the best
21 measurement (with 68% confidence level of χ^2 distribution), were considered acceptable. Projections
22 of the contour lines (with a contour value of 2.298) on the n and k plane gave the standard errors Δn
23 and Δk , respectively (Dinar et al., 2008; Zhao et al., 2014a).

25 3.2 Chemical apportionment of aerosol optical properties

26
27 Chemical apportionment of light extinction of $PM_{1.0}$ was determined with a revised IMPROVE
28 (Interagency Monitoring of Protected Visual Environments) algorithm (Pitchford et al., 2007).
29 Although the IMPROVE algorithm is a simplified predictor of extinction, it is nevertheless a useful

1 tool to estimate the contribution of different particle components to haze levels (Pitchford et al.,
 2 2007). Light extinction at $\lambda = 550$ nm can be estimated by multiplying the mass concentrations by
 3 component-specific mass extinction efficiencies (MEEs) of each of seven major components: sulfate
 4 (assumed to be ammonium sulfate), nitrate (assumed to be ammonium nitrate), organic mass (OM,
 5 based on the measured mass concentration of organic carbon, OC), elemental carbon (EC), fine soil,
 6 sea salt (chlorine, Cl), and coarse mass (the differences between PM_{10} and $PM_{2.5}$ mass concentration).
 7 It can be expressed by the following (Pitchford et al., 2007):

$$\begin{aligned}
 \alpha_{ext,550nm} \approx & 2.2 \times f_s(RH) \times [\text{Small Sulfate}] + 4.8 \times f_L(RH) \times [\text{Large Sulfate}] \\
 & + 2.4 \times f_s(RH) \times [\text{Small Nitrate}] + 5.1 \times f_L(RH) \times [\text{Large Nitrate}] \\
 & + 2.8 \times [\text{Small Organic Mass}] + 6.1 \times [\text{Large Organic Mass}] \\
 & + 10 \times [\text{Elemental Carbon}] + 1 \times [\text{Fine Soil}] \\
 & + 1.7 \times f_{ss}(RH) \times [\text{Sea Salt}] + 0.6 \times [\text{Coarse Mass}] \\
 & + \text{Rayleigh scattering (site specific)} + 0.33 \times [\text{NO}_2(\text{ppb})]
 \end{aligned} \tag{3}$$

9 where $f(RH)$ is the water growth factor of inorganic components, $f_s(RH)$ and $f_L(RH)$ are the water
 10 growth factors for the small and large particle size modes for sulfate and nitrate, respectively, and
 11 $f_{ss}(RH)$ is the hygroscopic growth factor for sea salt.

12 The large and small parts are defined by the IMPROVE formula as (Pitchford et al., 2007; Cao
 13 et al., 2012):

$$\begin{aligned}
 [\text{Large X}] &= [\text{Total X}]^2/20, \text{ for } [\text{Total X}] < 20 \mu\text{g m}^{-3} \\
 [\text{Large X}] &= [\text{Total X}], \text{ for } [\text{Total X}] \geq 20 \mu\text{g m}^{-3} \\
 [\text{Small X}] &= [\text{Total X}] - [\text{Large X}]
 \end{aligned} \tag{4}$$

17 where X = sulfate, nitrate or OM. The concentration of ammonium sulfate ($[(\text{NH}_4)_2\text{SO}_4]$) was 1.375
 18 times the sulfate concentration ($[\text{SO}_4^{2-}]$), and the ammonium nitrate ($[\text{NH}_4\text{NO}_3]$) was 1.29 times the
 19 nitrate concentrations ($[\text{NO}_3^-]$). The OM concentration was estimated by multiplying the reported OC
 20 concentration by a factor of 1.6 (Turpin and Lim, 2001). The sea salt mass concentration was
 21 estimated by multiplying the Cl mass concentration by a factor of 1.8. The ammonium cation was
 22 not used directly in the IMPROVE algorithm. It was assumed to be fully neutralized by SO_4^{2-} and
 23 NO_3^- and treated as ammonium sulfate ($(\text{NH}_4)_2\text{SO}_4$) and ammonium nitrate (NH_4NO_3), respectively.

24 The revised IMPROVE algorithm above was parameterized for atmospheric aerosol extinction at
 25 $\lambda = 550$ nm. In this study, the optical properties of $PM_{1.0}$ were measured at $\lambda = 470$ nm. The
 26 IMPROVE algorithm needs to be refined to better represent the chemical apportionment of light
 27 extinction for $PM_{1.0}$ particles. Since dry $PM_{1.0}$ aerosols were measured, the coarse mass and the

1 hygroscopic increase of inorganic component were ignored for the inputs of the IMPROVE
2 algorithm. The fine soil component was also left out in apportioning the extinction coefficient due to
3 its small fraction of PM_{1.0} particles during wintertime in Beijing (K. Sun et al., 2014).

4 Under the assumptions of the IMPROVE algorithm (in which particles are treated as separate
5 entities), the difference in the wavelength will only affect the dry mass extinction efficiency terms.
6 We modified the MEE terms in equation (3) of each individual particle components with a scaling
7 factor so as to be directly comparable to measurements at $\lambda = 470$ nm. The scaling factor was the
8 ratio of the MEEs of each species at $\lambda = 470$ nm and $\lambda = 550$ nm calculated with Mie theory from the
9 literature reported complex refractive index (Table S1 in the Supplement) and the measured mean
10 number size distribution. Further details are given in the Supplement, Section S2. The dry mass
11 extinction efficiencies of inorganic mass (including sulfate, nitrate and sea salt), organic mass, and
12 elemental carbon for the input of the IMPROVE formula at $\lambda = 470$ nm should accordingly be scaled
13 by factors of 1.31, 1.30 and 1.08, respectively. The modified IMPROVE function for PM_{1.0}
14 extinction at $\lambda = 470$ nm can be rewritten as following:

$$\begin{aligned} \alpha_{ext,470nm,PM_{1.0}} \approx & 2.88 \times [\text{Small Sulfate}] + 6.29 \times [\text{Large Sulfate}] \\ & + 3.14 \times [\text{Small Nitrate}] + 6.68 \times [\text{Large Nitrate}] \\ & + 3.64 \times [\text{Small Organic Mass}] + 7.93 \times [\text{Large Organic Mass}] \\ & + 10.8 \times [\text{Elemental Carbon}] + 2.23 \times [\text{Sea Salt}] \end{aligned} \quad (5)$$

16 The PM_{1.0} mass concentration can be reconstructed as the sum of its major chemical components
17 (Pitchford et al., 2007):

$$\begin{aligned} \text{Reconstructed mass}_{PM_{1.0}} &= [(\text{NH}_4)_2\text{SO}_4] + [\text{NH}_4\text{NO}_3] + [\text{SS}] + [\text{OM}] + [\text{EC}] \\ &= 1.375 \times [\text{SO}_4^{2-}] + 1.29 \times [\text{NO}_3^-] + 1.8 \times [\text{Cl}^-] + 1.6 \times [\text{OC}] + [\text{EC}] \end{aligned} \quad (6)$$

20 3.3 Mass scattering and absorption efficiencies

21
22 Mass scattering (MSE) and absorption (MAE) efficiencies are the key parameters in climate and
23 chemical transport models for estimating radiative forcing and apportioning chemical extinction
24 budgets (Bates et al., 2006; Malm and Hand, 2007). MSE and MAE (both conventionally in units of
25 $\text{m}^2 \text{g}^{-1}$) are defined as the ratio of the light scattering and absorption coefficients (Mm^{-1}) to the
26 aerosol volume mass concentration ($\mu\text{g m}^{-3}$), respectively.

$$\text{MSE (MAE)} = \frac{\alpha_{\text{scat,abs}}}{M} \quad (7)$$

Knowledge of the MSEs and MAEs of each component of atmospheric aerosol is helpful for accurate source apportionment and for estimating radiative forcing in climate modes. The simplest method for computing MSE is by direct measurement of aerosol scattering coefficient and the mass concentration. The average MSE is estimated either by dividing the average α_{scat} by the average mass concentration or from the slope of a linear regression of α_{scat} and M (Hand and Malm, 2007). The MAE is calculated similarly.

In this study, the MSEs and MAEs of $\text{PM}_{1.0}$ were estimated from the slope of a linear regression of $\alpha_{\text{scat,abs}}$ and M (each data point with 3 min time resolution). The $\alpha_{\text{scat,abs}}$ was directly measured with the cavity-enhanced albedometer with high time resolution, and M was calculated from the average density ($\bar{\rho}$) and the volume concentrations ($V(D_p)$) measured with the SMPS ($M = \bar{\rho} \int V(D_p) dD_p$). The average density was calculated from $\bar{\rho}^{-1} = \sum_j \rho_j^{-1} X_j$, where ρ_j is the density of each chemical component (see Table S1 in the Supplement), X_j is the mass concentration ratio of each species to the total $\text{PM}_{1.0}$ concentration (reconstructed with equation (6)) measured from filter samples with a time resolution of 12 h sample⁻¹.

4 Results and discussion

An overview of the measurement results of the aerosol optical properties, size distribution, and chemical composition of $\text{PM}_{1.0}$ particles is shown in Table 1 and Fig. 2. During the campaign, the measured aerosol extinction ($\alpha_{\text{ep},470}$), scattering ($\alpha_{\text{sp},470}$), and absorption coefficient ($\alpha_{\text{ap},470}$) ranged from 0.6–1165, 0.1–1150 and 0–276 Mm^{-1} , respectively. The time profiles of these properties also showed several periods during which the particle concentration would steadily build up, before rapid dissipation and return to fewer and smaller particles.

We present our results as follows: Firstly, selected periods are investigated in detail for showing the process of haze formation, development and decline. The extensive optical properties (extinction, scattering, and absorption coefficients) and intensive optical properties (SSA and effective CRI) are presented for these periods. Secondly, the diurnal variations of aerosol size distribution, optical

1 properties and chemical composition on different pollution days during the campaign are considered.
2 Chemical apportionment of aerosol extinction is then studied based on the modified IMPROVE
3 algorithm. And finally, the MSE and MAE of PM_{1.0} particles are presented for clear, slightly polluted,
4 and polluted days.

5

6 **4.1 Temporal variations of optical properties during selected air pollution episodes**

7

8 The temporal variations of aerosol particle number and surface size distribution, aerosol
9 extinction, scattering, absorption coefficients, ω_{470} , and the retrieved **effective** CRIs from 22 to 24
10 November 2014 are presented in Fig. 3. The corresponding temporal wind direction and speed are
11 shown in the upper panel of Fig. 3, **while temperature, relative humidity, pressure, and**
12 **concentrations of pollutant gases (SO₂, NO₂, O₃, and CO) are shown in Fig. S3 in the Supplement.**
13 The time series of PM_{1.0} particle number distribution during the episode varied with meteorology and
14 the sources of pollutants. To emphasize the variation of these parameters during the episode, the
15 extended air pollution episode was divided into six shorter periods. The statistical analyses of these
16 periods are summarized in Table 2.

17 24 h back trajectories starting at 200 m a.g.l. in Huairou site calculated every 4 h (at 02:00, 6:00,
18 10:00, 14:00, 18:00 and 22:00 LT) are shown in the lower panel of Fig. 4
19 (<http://ready.arl.noaa.gov/HYSPLIT.php>). The trajectories from the northerly direction were clean air
20 masses with high transport heights and long transport pathways; trajectories from the southerly
21 direction were mainly polluted air masses with low transport heights and short transport pathways.

22 According to the regulatory classification of the atmospheric pollution level, these six periods
23 can be divided into two categories: clear day (22:00 LT 21 November–10:00 LT 22 November) and
24 polluted day (10:00 LT 22 November–22:00 LT 22 November, 22:00 LT 22 November–10:00 LT 23
25 November, 10:00 LT 23 November–22:00 LT 23 November, 22:00 LT 23 November–10:00 LT 24
26 November). **The mean value of the total mass concentration on clear days was 9.49 $\mu\text{g m}^{-3}$, and the**
27 **mean fractional contributions of OM, nitrate, and sulfate were 56% (5.32 $\mu\text{g m}^{-3}$), 12% (1.12 $\mu\text{g m}^{-3}$),**
28 **and 14% (1.34 $\mu\text{g m}^{-3}$), respectively. On polluted days, the mean value of the total mass**
29 **concentration was 41.64 $\mu\text{g m}^{-3}$ with fractional contributions of 44% OM (18.47 $\mu\text{g m}^{-3}$), 22% nitrate**
30 **(9.30 $\mu\text{g m}^{-3}$), and 11% sulfate (4.54 $\mu\text{g m}^{-3}$). In summary, in going from clear to polluted days, the**

1 fractional contribution of OM to the total mass decreased by 12%, whereas the fraction of nitrate
2 almost doubled and that of sulfate decreased slightly. Organic matter was the largest contributor to
3 $PM_{1.0}$. The significant increase in the concentration and fractional contribution to $PM_{1.0}$ extinction
4 coefficient of inorganic species, particularly nitrates (discussed in Section 4.3), indicate that
5 inorganic species become more important during haze, an observation which is consistent with
6 previously measurements during an extreme haze episode in Beijing in January 2013 (Wang et al.,
7 2015). The difference between sulfate and nitrate likely reflects the different sources and formation
8 mechanisms for sulfate and nitrate aerosols (G. J. Zheng et al., 2015).

9 In the selected haze episode, these six periods show variations in the $PM_{1.0}$ size distribution and
10 the extensive optical properties of particles in the process of haze formation, development and
11 decline. The evolution of intensive optical properties was related to the variation of $PM_{1.0}$ chemical
12 components.

14 **Period 1: First traffic-dominated pollution period (05:40–10:00 LT 22 November)**

16 Relatively small, light absorbing particles dominated this period. The mean diameter of the
17 number size distribution was 56 ± 6 nm, and the average number and surface concentration were 2.1
18 $\pm 0.8 \times 10^4$ particle cm^{-3} and $3.7 \pm 1.5 \times 10^8$ $nm^2 cm^{-3}$, respectively. The mean values of $\alpha_{ep,470}$, $\alpha_{sp,470}$,
19 and $\alpha_{ap,470}$ were 56 ± 24 , 44 ± 10 and 12 ± 6 Mm^{-1} , respectively. The ω_{470} , real and imaginary part of
20 effective CRI (n, k) were 0.79 ± 0.03 , 1.38 ± 0.06 and 0.03 ± 0.02 , respectively.

21 During this period, winds were typically from the northeast; the trajectory indicated that the air
22 masses came from cleaner air to the north and carried pollutants from northeast areas to the
23 observation site, with concentrations of small, light absorption particles increasing. These clean air
24 masses showed a relatively large contribution from traffic emissions. Lower values of the SSA were
25 found during the rush hour, in common with other studies that have similarly found minimum SSA
26 values during the morning traffic rush hour (Garland et al., 2008; Lyamani et al., 2010).

28 **Period 2: New particle formation period (12:40–15:00 LT 22 November)**

30 This period started with clean atmospheric conditions and was characterized by the formation

1 and growth of small particles. The mean diameter of the number size distribution was 25 ± 4 nm and
2 the mean values of $\alpha_{ep,470}$, $\alpha_{sp,470}$ and $\alpha_{ap,470}$ were 17 ± 5 , 16 ± 5 and 1.0 ± 0.4 Mm^{-1} , respectively.
3 The mean values of ω_{470} , n and k were 0.94 ± 0.03 , 1.40 ± 0.06 and 0.008 ± 0.005 , respectively.
4 These values indicated that optical extinction in these newly formed particles was dominated by
5 scattering, although it should be noted that the uncertainties in the ω_{470} values are larger under these
6 conditions of low scattering and extinction.

7 For Period 2, the air masses came from the north with clean air, but their reduced height resulted
8 in entrainment of surface aerosols and transport to the observation site. The transport of clean, fresh
9 air resulted in sharply decreased pollutant levels and promoted new particle formation. Takegawa et
10 al. (2009) and Guo et al. (2014) showed that newly formed aitken mode particles were mainly
11 composed of sulfate and organic matter, indicating that most components were absolute scattering
12 species. In this case, the values of SSA and k should be close to 1 and 0, respectively. The retrieved
13 values of SSA (0.94 ± 0.03) and k (0.008 ± 0.005) matched these expectations and indicate that the
14 newly formed particles were predominantly scattering species.

15

16 **Period 3: Accumulated pollution period (15:30 LT 22 November–08:00 LT 23 November)**

17

18 This period was characterized by the dominance of larger accumulation mode particles for
19 several hours. The mean diameter of number and surface size distribution was 106 ± 16 and 229 ± 16
20 nm, respectively, which increased slowly from 15:30 LT (with a minimum value of 60 and 205 nm)
21 to 21:40 LT (with a maximum value of 131 and 248 nm) except for a valley from 17:20–18:00 LT
22 that coincided with the afternoon rush hour. The mean values of $\alpha_{ep,470}$, $\alpha_{sp,470}$ and $\alpha_{ap,470}$ were $179 \pm$
23 69 , 151 ± 57 and 28 ± 12 Mm^{-1} , respectively.

24 In the first part of the period, the winds slowed down and turned to the south. These conditions
25 favored accumulation of local pollutants (including primary emissions and secondary productions)
26 and transportation of pollutants from southern areas. Later on, the wind speed increased and the
27 direction changed to the southeast. The accumulation of pollutants brought about the formation of
28 haze. During the process, the number concentration increased about 1.7 times from 1.2×10^4 to
29 2.0×10^4 particle cm^{-3} , and the surface concentration increased about 1.3 times from 3.2×10^8 to
30 10.3×10^8 $nm^2 cm^{-3}$, leading to large values of $\alpha_{ep,470}$ ($285 Mm^{-1}$), $\alpha_{sp,470}$ ($235 Mm^{-1}$) and $\alpha_{ap,470}$ (50

1 Mm⁻¹). The wind speed eventually decreased and the wind direction changed, first to northeastern,
2 and then to southeastern directions. Another major peak in the extinction occurred during this period
3 when a large number of small size particles were observed. The mean values of ω_{470} , and the real
4 part and imaginary part of the **effective** CRI were 0.85 ± 0.01 , 1.39 ± 0.04 and 0.02 ± 0.006 ,
5 respectively. Clearly, the air masses from northeast areas carried appreciable numbers of small, light
6 absorbing particles.

7

8 **Period 4: Combined pollution period (08:30–12:00 LT 23 November)**

9

10 **For Periods 3 and 4, the shorter transport pathway of air masses suggested that the composition**
11 **was dominated by local emissions, including primary emissions and secondary formation.** Large
12 numbers of small, light absorbing particles were seen during period 4, which coincided with the
13 morning rush hour. The mean diameter of the number and surface size distribution was 105 ± 16 and
14 251 ± 15 nm, respectively, and $\alpha_{ep,470}$, $\alpha_{sp,470}$ and $\alpha_{ap,470}$ were 405 ± 60 , 321 ± 42 and 84 ± 22 Mm⁻¹,
15 respectively. The mean values of ω_{470} and the imaginary part of the **effective** CRI were 0.79 ± 0.03
16 and 0.034 ± 0.008 , respectively, which were similar to the values in the first traffic-dominated
17 pollution period. The real part of the **effective** CRI (1.40 ± 0.03) was **similar to** that of the earlier
18 traffic-dominated pollution period **within the stated uncertainties.** During the period, weak winds
19 from northern directions transported polluted air to the observation site and resulted in higher
20 concentrations and a greater influence of light absorbing particles. The accumulation of original and
21 newly discharged primary pollutants led to sharp variations in the aerosol size distribution and
22 extensive optical properties. Variations in the aerosol intensive optical properties were slight.

23

24 **Period 5: Particle aggregation and removal period (12:30 LT 23 November–07:30 LT 24**

25 **November)**

26

27 High extinction values were observed over this period, with a gradual increase and then decrease
28 in extinction, scattering, and absorption. The mean values of $\alpha_{ep,470}$, $\alpha_{sp,470}$ and $\alpha_{ap,470}$ were 330 ± 110 ,
29 283 ± 94 and 46 ± 16 Mm⁻¹, respectively. The mean values of ω_{470} , n and k were 0.86 ± 0.01 , $1.44 \pm$
30 0.03 , and 0.02 ± 0.01 , respectively, which were larger than the values of the period 4 (although

1 within the combined uncertainties).

2 Air mass trajectories indicate that the airflow started over the Beijing city area and passed over
3 the southwestern direction of the observation site. Air masses following this short path would bring
4 surface air pollutants to the Huairou site and contribute to the formation of serious haze. In the first
5 part of the period, winds from the north moderated and the wind direction changed to the northeast,
6 favoring accumulation of local pollutants. Later on, the wind changed to the southeast, with
7 pollutants from the south contributing to the formation of serious haze. Particles dispersed later after
8 the wind speed increased and its direction became northeasterly. Both the mean diameter of the
9 number and surface size distribution (124 ± 19 and 263 ± 11 nm) and n were larger in this period
10 than in the other five periods. The light scattering efficiency increased with the increment of the
11 particle size.

13 **Period 6: Second traffic-dominated pollution period (08:00–11:10 LT 24 November)**

14
15 This period corresponded to the morning rush hour on 24 November. The mean values of $\alpha_{\text{ep},470}$,
16 $\alpha_{\text{sp},470}$ and $\alpha_{\text{ap},470}$ were 80 ± 42 , 64 ± 34 and 16 ± 8 Mm^{-1} , respectively, and were slightly larger than
17 in the first traffic-dominated pollution period. The mean values of ω_{470} (0.78 ± 0.04), n and k ($1.40 \pm$
18 0.04 and 0.04 ± 0.02) were comparable to the earlier traffic period. The mean diameter of the number
19 and surface size distribution was 64 ± 12 and 226 ± 14 nm, respectively, and a larger n value was
20 found. In this period, strong winds from the north transported clean air to the observation site,
21 leading to lower particle concentrations and a greater influence of fresh local emissions.

23 **4.2 Aerosol size distributions, optical properties, chemical composition and light extinction** 24 **apportionment on different air pollution days**

25
26 Averages and standard deviations of the observed particle properties are summarized in Table 1
27 after grouping data into the different air quality classes. There are obvious differences of the
28 campaign average number and surface size distribution of $\text{PM}_{1.0}$ for the three different pollution
29 categories (Fig. 5a). For clear days, the mean particle number size distributions fitted by a mono-log
30 normal function was around 41 nm. Bimodal distributions were observed on slightly polluted and

1 polluted days with modes centered at 38 and 105 nm (slightly polluted periods) and at 38 and 151 nm
2 (polluted periods). The mode of the number size distributions exhibits the expected displacement
3 toward the accumulation mode with increasing levels of particulate matter.

5 **Chemical composition**

7 Table 1 and Fig. 5b show the mean **mass concentration** values and the mean percentile
8 compositions of observed chemical compositions of PM_{1.0} particles under different pollution levels.
9 The contribution of sulfate, nitrate and ammonium to the observed PM_{1.0} mass concentration
10 increased strongly on polluted compared to clear days (from 34 to 44%). Similar trends were
11 observed for PM_{2.5} and NR-PM_{1.0} during the January 2013 severe haze events in Beijing (Y. L. Sun
12 et al., 2014; Tao et al., 2015; G. J. Zheng et al., 2015).

13 On average, OM, nitrate, sulfate, ammonium, chloride and EC comprised 46.3% ($13.3 \pm 11.1 \mu\text{g}$
14 m^{-3}), 18.0% ($5.2 \pm 5.5 \mu\text{g} \text{m}^{-3}$), 11.6% ($3.3 \pm 3.5 \mu\text{g} \text{m}^{-3}$), 10.3% ($3.0 \pm 3.6 \mu\text{g} \text{m}^{-3}$), 5.3% (1.5 ± 1.9
15 $\mu\text{g} \text{m}^{-3}$) and 3.9% ($1.1 \pm 0.9 \mu\text{g} \text{m}^{-3}$) of observed PM_{1.0}, respectively. The organic mass was the
16 largest proportion in PM_{1.0} particles, and the contribution of nitrate was larger than that of sulfate.
17 Compared to summer, the **mass** contribution of organics was significantly higher during winter, and
18 primary organic aerosol dominated during the coal heating season (Sun et al., 2013). Huang et al.
19 (2014) reported that secondary organic aerosol (SOA) contributed 26% of PM_{2.5} in Beijing in the
20 January 2013 severe haze events, and indicated the dominant effect of fossil fuel SOA formation in
21 Beijing regions. Compared to sulfate, the fractional composition of nitrate and ammonium aerosol
22 increased under high levels of pollution. The differences may be due to both photochemical and
23 aqueous processing which are important in nitrate formation (Wang et al., 2015) and may play a
24 more important role in sulfate formation during wintertime (Sun et al., 2013).

26 **Optical properties**

28 There was no obvious correlation between extensive optical properties and wind direction (Fig.
29 S4). With increasing pollutant level, the extensive optical properties ($\alpha_{\text{ep},470}$, $\alpha_{\text{sp},470}$ and $\alpha_{\text{ap},470}$)
30 increased strongly, in accordance with the expected, strong dependence of particle size on light

1 scattering. In contrast, changes in the intensive optical properties (ω_{470}) were more modest. The
2 optical measurement data are presented as histograms of the relative frequency of occurrence of
3 $\alpha_{ep,470}$, $\alpha_{sp,470}$, $\alpha_{ap,470}$ and ω_{470} (Fig. 6). Approximately 71% of extinction and scattering coefficients
4 values were lower than 200 Mm^{-1} and nearly 80% of absorption coefficient values were located in
5 the range of $1.5\text{--}50 \text{ Mm}^{-1}$. Approximately 90% of the ω_{470} values fell into the range of 0.70–0.97.
6 Compared with polluted days, the frequency distribution of the SSA showed similar patterns, and the
7 average values were similar on clear and slightly polluted days.

8 The Huairou site is a new suburban site at which aerosol optical properties have not previously
9 been reported. To put our observations at Huairou in context, the scattering and absorption
10 coefficients and SSA observed in this campaign are compared in Table 3 to those at other locations
11 (urban, suburban, and rural sites). As would be expected given the high concentrations of particulate
12 matter in much of China, the mean $\alpha_{sp,470}$ value at Huairou was considerably higher than values
13 observed in America and Europe, including the Los Angeles basin measurements in Pasadena
14 (Thompson et al., 2012) and the urban site of Granada (Titos et al., 2012). Within China, the Huairou
15 values for scattering and absorption were higher than in Shanghai (Li et al., 2013) and similar to the
16 urban site of Guangzhou in China (Garland et al., 2008). Compared with other non-urban polluted
17 sites in China, both $\alpha_{sp,470}$ and $\alpha_{ap,470}$ at Huairou were lower than Xinken (Cheng et al., 2008), Yufa
18 (Garland et al., 2009) and much lower than Xianghe (Li et al., 2007). Moreover, the $\alpha_{sp,470}$ values
19 were comparable to those observed at Shangdianzi, an atmospheric background site located $\sim 150 \text{ km}$
20 northeast of the urban center of Beijing (Yan et al., 2008). The average value of $\alpha_{ap,470}$ at Huairou
21 was lower than those seen at other urban and suburban locations in China, with the exceptions of
22 Guangzhou (reflecting the lower SSA values observed in Huairou) and the rural site of Shangdianzi.

23 The regional differences in SSA can be considered in terms of the different sources of particles,
24 including local primary emissions, transport emissions and secondary aerosol formations. The
25 average value of ω_{470} at Huairou was 0.80 ± 0.08 , which was lower than suburban sites in Xinken
26 (0.83 ± 0.05), Xianghe ($0.81\text{--}0.85$) and Yufa (0.86 ± 0.07), and rural sites in Shangdianzi ($0.88 \pm$
27 0.05), and Pasadena (0.92 ± 0.08). Compared to urban sites, the Huairou SSA was similar to
28 observations in Beijing (0.80 ± 0.09) (He et al., 2009), but considerably higher than in Shanghai
29 (0.70 ± 0.07) (Li et al., 2013) and Granada (0.71 ± 0.07) (Titos et al., 2012). The lower SSA values
30 probably arose from the higher contribution of vehicular emissions in Shanghai (Zhou et al., 2009)

1 and both traffic emissions and a higher mass fraction of light absorbing particles caused by fuel-oil
2 combustion in Granada (Titos et al., 2012).

3 The diurnal variations of hourly averaged extinction, scattering, absorption coefficient and SSA
4 on clear, slightly polluted and polluted days are presented in Fig. 7. Broadly similar patterns were
5 observed for the extensive optical properties for different pollutant levels. Extinction ($\alpha_{ep,470}$) and
6 scattering ($\alpha_{sp,470}$) tended to be lower during daytime and higher at night. Emissions associated with
7 morning rush hour are apparent in the aerosol optical properties. $\alpha_{ep,470}$ and $\alpha_{sp,470}$ increased slowly
8 in the morning (07:00–09:00 LT) to peak values at 09:00 LT, indicating significant emission and
9 formation of particles during this period; these properties then decreased slowly until about 14:00 LT.
10 The maximum values of $\alpha_{ap,470}$ occurred during the traffic rush hour and could be attributed to direct
11 emissions of light absorbing species from vehicles. We note that the increase in $\alpha_{ap,470}$ from 06:00 to
12 the maximum at 08:00 to 09:00 LT varied from 10 to 20 Mm^{-1} and was quite consistent across
13 different pollutant days. This observation suggests that the number and type of particles emitted
14 during this time period is not strongly influenced by pre-existing pollutant levels; however, this is
15 what would be expected for relatively constant daily emissions from traffic.

17 Chemical apportionment of aerosol optical properties

18
19 Over the past years, the chemical apportionment of α_{ep} or α_{sp} has been conducted in both urban
20 and non-urban regions (Malm et al., 1994; Watson, 2002; Cheung et al., 2005; Malm and Hand, 2007;
21 Yang et al., 2007; Tao et al., 2009; Cao et al., 2012; Han et al., 2014; Tao et al., 2014a; Cheng et al.,
22 2015). Ammonium sulfate was generally the largest contributor to $PM_{2.5}$ or PM_{10} α_{ep} , with a range
23 from 20–50%. However, fewer studies have been reported of the chemical contribution of different
24 chemical components to the extinction of $PM_{1.0}$ under different pollution levels. Studies in other
25 Chinese megacities, such as Shanghai (Cheng et al., 2015) and Guangzhou (Tao et al., 2014b), and
26 data from US monitoring sites show that the revised IMPROVE algorithm underestimates the $PM_{2.5}$
27 extinction under high aerosol loading but overestimates the values under low aerosol loading. The
28 underestimation and overestimation ratios in different studies ranged from -11 to -26 % and +25 to
29 +54 %, respectively (Cheng et al., 2015).

30 In this work, $\alpha_{ep,470}$ of $PM_{1.0}$ particles was reconstructed using the modified IMPROVE

1 algorithm based on the measured concentrations of each composition (Fig. 8a), which correlated well
2 with the measured $\alpha_{ep,470}$ ($R^2 = 0.96$) during this campaign (Fig. 8c). With improved mass extinction
3 efficiencies, the agreement between the measured and calculated $PM_{1.0}$ extinctions is good (with a
4 slope of 1.04 ± 0.04) when the measured extinction coefficient is lower than $300 Mm^{-1}$ (as shown in
5 the insert of Fig. 8c). When the observed extinction coefficients are larger than $300 Mm^{-1}$, the
6 reconstructed values of the modified IMPROVE algorithm were 16% lower than observed values
7 (calculated from the average of the ratios of the measured extinction to the reconstructed extinction
8 for all points $> 300 Mm^{-1}$). The modified IMPROVE algorithm for $PM_{1.0}$ at $\lambda = 470$ nm represents
9 the chemical apportionment of light extinction quite well. The reconstructed $PM_{1.0}$ mass
10 concentration (Fig. 8b) using the modified IMPROVE algorithm was well correlated with the
11 measured $PM_{1.0}$ mass concentration (the summation of the concentrations of eight water-soluble ion
12 compositions and carbon concentration (including elemental carbon, [EC], and organic mass,
13 $1.6 \times [OC]$)) ($R^2 = 0.99$, slope = 1.00, intercept = 0.28) (Fig. 8d), indicating that the modified
14 IMPROVE algorithm can be used to estimate the chemical apportionment for extinction in this
15 campaign.

16 The average fractional contributions of each chemical component of dry $PM_{1.0}$ extinction
17 coefficient with respect to different pollution levels are shown in Fig. 9. The optical extinction
18 caused by OM, ammonium nitrate, ammonium sulfate, elemental carbon and sea salt accounted for
19 57.9, 17.8, 12.5, 8.6 and 3.2 % of the reconstructed $PM_{1.0}$ extinction in this campaign, respectively.
20 The contribution of chemical compositions to aerosol extinction depends mainly on their mass
21 concentrations. The mass concentrations of OM, ammonium nitrate, ammonium sulfate, element
22 carbon and sea salt accounted for 50.4, 21.2, 16.8, 4.2 and 7.4 % of the reconstructed $PM_{1.0}$ mass
23 concentrations, respectively. The organic constituents comprised a large fraction of $PM_{1.0}$ mass
24 concentration, consistent with previous studies (Yao et al., 2010; Sun et al., 2013).

25 OM therefore made the largest contribution to the extinction of $PM_{1.0}$ particles in this study. The
26 relative contribution of OM (58 %) to the total extinction reported here was comparable to that
27 previously reported in Beijing (54 %) during an extreme haze episode in January 2013 for $PM_{1.0}$
28 scattering (Wang et al., 2015), and in Shenzhen (45 %) in the winter of 2009 for $PM_{2.5}$ extinction
29 (Yao et al., 2010). The contribution of organics in Beijing increases significantly during the winter
30 coal heating season (Sun et al., 2013). Emissions from the large number of vehicles in the

1 mega-cities of China also contributes significantly to organic aerosol (Huang et al., 2014). From
2 clear days to slightly polluted days, the relative contribution of organic mass to light extinction
3 increased by 7 %, which may due to an increasing contribution of secondary organic aerosol (SOA)
4 (Huang et al., 2014). The concentrations of nitrate and ammonium aerosol increased under high
5 levels of pollution, and the relative contribution of ammonium nitrate to PM_{1.0} light extinction
6 increased by 6.7 % under these conditions (Wang et al., 2015). Various anthropogenic emissions,
7 especially coal consumption, biomass burning and vehicle exhaust, result in many sources of EC in
8 the NCP. Although EC only comprised about 4 % of PM_{1.0} mass concentration, it contributed
9 appreciably to PM_{1.0} extinction owing to its high absorption efficiency.

11 4.3 MSE and MAE of PM_{1.0}

13 Figure 10 shows the relationship between the scattering and absorption coefficients and PM_{1.0}
14 mass concentrations under different pollution levels. The PM_{1.0} mass concentrations were determined
15 by multiplying the volume concentrations with the volume-weighted mass density of each filter
16 sample (Hasan and Dzubay, 1983). The scattering and (to a lesser extent) the absorption coefficients
17 were generally well correlated with the PM_{1.0} mass concentrations and have small y-intercepts. (The
18 larger deviation of the y-intercept on polluted days likely stems from the smaller number of low mass
19 concentration observations on these days.)

20 The derived PM_{1.0} average mass scattering and absorption efficiencies during the campaign were
21 3.60 and 0.70 m² g⁻¹, respectively (Fig. 10d). Statistical uncertainties from the slope of the regression
22 are misleadingly small and have been omitted in the reported MSE and MAE values. The MSE and
23 MAE values are smaller than those observed by Garland et al. (2008) from suburban Guangzhou in
24 July 2006 (where the PM_{1.0} mass scattering and absorption efficiency calculated with assuming an
25 average effective density of ammonium sulfate (1.7 g cm⁻³) were 4.13 and 1.09 m² g⁻¹, respectively),
26 the value of PM_{2.5} at λ = 520 nm obtained in urban Beijing (4.8 m² g⁻¹) during wintertime (Tao et al.,
27 2015), and in Chengdu and Guangzhou (3.9 m² g⁻¹) (Tao et al., 2014a, b). The derived mass
28 extinction efficiency is 4.30 m² g⁻¹, which was comparable to the reported values during Aerosols
29 1999 (4.1–5.4 m² g⁻¹) (Quinn et al., 2001) and INDOEX 1999 (4.0–5.6 m² g⁻¹) (Quinn et al., 2002).

30 In this work, the MSE of PM_{1.0} was 4.16 m² g⁻¹ during polluted days, which was 34% higher

1 than that during the slightly polluted days ($3.11 \text{ m}^2 \text{ g}^{-1}$) and 75% higher than that during the clear
2 days ($2.38 \text{ m}^2 \text{ g}^{-1}$) (Fig. 10a–c). The variability in MSE is typically more dependent on mass size
3 distribution than on density or refractive index (Hand and Malm, 2007). As shown in Fig. 5(a), the
4 particle diameter increased significantly with high aerosol mass concentrations. The MSEs in this
5 work increased consistently with pollution level, primarily because larger particles scatter light more
6 efficiently. Cheng et al. (2015) showed that the MSEs of ammonium nitrate, ammonium sulfate and
7 organic matter increased rapidly with increasing mass concentration at lower aerosol loadings, while
8 the MSEs of ammonium nitrate and ammonium sulfate fluctuated in a narrow range under high
9 aerosol loading conditions when the MSE of organic matter is slightly smaller. One recent study
10 (Tao et al., 2015) showed that the MSE was determined by the proportions of the dominant chemical
11 components and their size distributions under different pollution levels. The MSEs in this work
12 increased consistently with the mass concentration of particles because of the relationship between
13 size and light scattering efficiency.

14 The observed MAEs of $\text{PM}_{1.0}$ were 0.61, 0.75, and $0.60 \text{ m}^2 \text{ g}^{-1}$ for clear, slightly polluted and
15 polluted days, respectively. At the same time, the EC fraction decreased with increasing pollution
16 level (clear days: $0.48 \pm 0.39 \mu\text{g m}^{-3}$ ($4.3 \pm 3.6 \%$), slightly polluted days: $1.18 \pm 0.59 \mu\text{g m}^{-3}$ ($4.0 \pm$
17 2.0%) and polluted days: $2.72 \pm 0.87 \mu\text{g m}^{-3}$ ($3.6 \pm 1.1\%$). As EC is the only absorbing species in the
18 modified IMPROVE algorithm, the extinction coefficients reconstructed using equation (5) can be
19 divided into two parts: absorption caused by EC and scattering caused by the other four groups. To
20 compare with the measurement results, the reconstructed $\text{PM}_{1.0}$ mass concentration was used for the
21 calculation of the reconstructed MSEs and MAEs of $\text{PM}_{1.0}$ particles (Fig. 11). The calculated MSEs
22 were 1.64, 1.58 and 1.43 times larger than the observed MSEs for clear, slightly polluted and
23 polluted days, respectively. In contrast, the calculated MAE values were 1.41, 1.67 and 1.54 times
24 smaller than the experimental results. MSEs increased with increasing pollution level in both
25 experimental and calculated results (the differences in measured and calculated MSE values were
26 -1.53 , -1.82 , and $-1.78 \text{ m}^2 \text{ g}^{-1}$, respectively), whereas for MAEs, the experimental and calculated
27 values increased in slightly polluted conditions, but decreased under polluted conditions (the
28 differences in the measured and calculated values were 0.18, 0.30, and $0.21 \text{ m}^2 \text{ g}^{-1}$, respectively).
29 Even though further improvement of the calculation method is necessary, the large difference of
30 MAE on slightly polluted days suggests aerosol absorption is incompletely represented. This

1 discrepancy may indicate the presence of other light absorbing components such as brown carbon,
2 BrC. Wang et al. (2013) have recently shown that BrC was the second-largest absorbing aerosol
3 constituent in Beijing (with a contribution of about 5 - 25%) and exhibits a clear seasonal variation
4 (dominates in late fall and winter, and extremely low in summer).

5 6 **5 Summary and conclusions**

7
8 $PM_{1.0}$ optical properties and composition at a suburban site near Beijing were measured during
9 the HOPE-J³A campaign. Six periods were investigated in detail to study the evolution of intensive
10 optical properties and chemical composition in $PM_{1.0}$ during an extended haze episode. Our analysis
11 reveals that the optical properties of aerosols change significantly during the evolution of haze.

12 New particle formation and primary emissions were apparent on clear days. The highest values
13 of ω_{470} and the lowest values of imaginary part of the **effective** CRI suggest that particle extinction
14 following new particle formation is dominated by scattering. During the formation of haze, both the
15 size and number concentration of atmospheric fine particles increased, which increased the light
16 scattering efficiency and the real component of the **effective** CRI. Traffic-dominated pollution
17 periods were characterized by small, light absorbing particles (e.g., black carbon), leading to the
18 lowest SSA and the highest imaginary component of the **effective** CRI. For the combined pollution
19 period, the accumulation of original and newly discharged primary pollutants led to sharp variations
20 in the aerosol size distribution and extensive optical properties.

21 The **mass concentrations** of sulfate, nitrate, and ammonium species were high during haze
22 episodes. **Organic matter was consistently the dominant constituent by mass of the observed aerosols,**
23 **and light extinction apportionment indicated that was it accordingly made the largest contribution to**
24 **the extinction of $PM_{1.0}$. Under polluted conditions, the proportion of inorganic components,**
25 **especially nitrate, was higher than under clean conditions and the contribution of inorganic**
26 **components to visibility degradation was significant.**

27 MSE increased consistently with the extent of pollution, whereas MAE increased with
28 increasing mass concentration in slightly pollution conditions but decreased under polluted
29 conditions. However, the EC fraction decreased with increasing pollution level, whereas the increase
30 of MAE under slightly polluted days may indicate a significant contribution of other species such as

1 brown carbon to the light absorption of the aerosol.

2

3

4 *Acknowledgements.* The authors wish thank to Zhouqing Xie at University of Science and
5 Technology of China for providing the meteorological data used in this paper and to Jun Tao and
6 Zejian Lin at South China Institute of Environmental Science for helpful discussion. This research
7 was supported by the National Natural Science Foundation of China (41330424), the Natural Science
8 Foundation of Anhui Province (1508085J03), the Key Research Program of the Chinese Academy of
9 Sciences (KJZD-EW-TZ-G06–01), and the China Special Fund for Meteorological Research in the
10 Public Interest (GYHY201406039). The support of the CaPPA project (“Chemical and Physical
11 Properties of the Atmosphere”), funded by the French National Research Agency through the
12 “Programme d’Investissement d’Avenir” (under contract ANR-10-LABX-005), is acknowledged.

13

14

15 **References**

16

17 Abo Riziq, A., Erlick, C., Dinar, E., and Rudich, Y.: Optical properties of absorbing and
18 non-absorbing aerosols retrieved by cavity ring down (CRD) spectroscopy, *Atmos. Chem.*
19 *Phys.*, 7, 1523–1536, doi:10.5194/acp-7-1523-2007, 2007.

20 Anderson, T. L., Charlson, R. J., Schwartz, S. E., Knutti, R., Boucher, O., Rodhe, H., and
21 Heintzenberg, J.: Atmospheric science. Climate forcing by aerosol – a hazy picture, *Science*,
22 300, 1103–1104, 2003.

23 Andersson, A., Deng, J., Du, K., Zheng, M., Yan, C., Skold, M., and Gustafsson, O.:
24 Regionallyvarying combustion sources of the January 2013 severe haze events over eastern
25 China, *Environ. Sci. Technol.*, 49, 2038–2043, doi:10.1021/es503855e, 2015.

26 Bahadur, R., Praveen, P. S., Xu, Y., and Ramanathan, V.: Solar absorption by elemental and brown
27 carbon determined from spectral observations, *P. Natl. Acad. Sci. USA*, 109, 17366–17371,
28 2012.

29 Bates, T. S., Huebert, B. J., Gras, J. L., Griffiths, F. B., and Durkee, P. A.: International Global
30 Atmospheric Chemistry (IGAC) project’s first aerosol characterization experiment (ACE 1):
31 overview, *J. Geophys. Res.*, 103, 16297–16318, doi:10.1029/97jd03741, 1998.

32 Bates, T. S., Anderson, T. L., Baynard, T., Bond, T., Boucher, O., Carmichael, G., Clarke, A., Erlick,
33 C., Guo, H., Horowitz, L., Howell, S., Kulkarni, S., Maring, H., McComiskey, A.,
34 Middlebrook, A., Noone, K., O’Dowd, C. D., Ogren, J., Penner, J., Quinn, P. K., Ravishankara,
35 A. R., Savoie, D. L., Schwartz, S. E., Shinozuka, Y., Tang, Y., Weber, R. J., and Wu, Y.:
36 Aerosol direct radiative effects over the northwest Atlantic, northwest Pacific, and North

- 1 Indian Oceans: estimates based on in-situ chemical and optical measurements and chemical
2 transport modeling, *Atmos. Chem. Phys.*, 6, 1657–1732, doi:10.5194/acp-6-1657-2006, 2006.
- 3 Cahill, J. F., Suski, K., Seinfeld, J. H., Zaveri, R. A., and Prather, K. A.: The mixing state of
4 carbonaceous aerosol particles in northern and southern California measured during CARES
5 and CalNex 2010, *Atmos. Chem. Phys.*, 12, 10989–11002, doi:10.5194/acp-12-10989-2012,
6 2012.
- 7 Cao, J., Chow, J. C., Lee, F. S. C., and Watson, J. G.: Evolution of PM_{2.5} measurements and
8 standards in the US and future perspectives for china, *Aerosol Air Qual. Res.*, 13, 1197–1211,
9 2013.
- 10 Cao, J. J., Wang, Q. Y., Chow, J. C., Watson, J. G., Tie, X. X., Shen, Z. X., Wang, P., and An, Z. S.:
11 Impacts of aerosol compositions on visibility impairment in Xi'an, China, *Atmos. Environ.*, 59,
12 559–566, doi:10.1016/j.atmosenv.2012.05.036, 2012.
- 13 Cheng, Y. F., Wiedensohler, A., Eichler, H., Su, H., Gnauk, T., Brüggemann, E., Herrmann, H.,
14 Heintzenberg, J., Slanina, J., Tuch, T., Hu, M., and Zhang, Y. H.: Aerosol optical properties
15 and related chemical apportionment at Xinken in Pearl River Delta of China, *Atmos. Environ.*,
16 30 42, 6351–6372, doi:10.1016/j.atmosenv.2008.02.034, 2008.
- 17 Cheng, Z., Jiang, J., Chen, C., Gao, J., Wang, S., Watson, J. G., Wang, H., Deng, J., Wang, B., Zhou,
18 M., Chow, J. C., Pitchford, M. L., and Hao, J.: Estimation of aerosol mass scattering
19 efficiencies under high mass loading: case study for the megacity of Shanghai, China, *Environ.*
20 *Sci. Technol.*, 49, 831–838, doi:10.1021/es504567q, 2015.
- 21 Cheung, H. C., Wang, T., Baumann, K., and Guo, H.: Influence of regional pollution outflow on the
22 concentrations of fine particulate matter and visibility in the coastal area of southern China,
23 *Atmos. Environ.*, 39, 6463–6474, doi:10.1016/j.atmosenv.2005.07.033, 2005.
- 24 **Chu, D. A., Kaufman, Y. J., Zibordi, G., Chern, J. D., Mao, J. T., Li, C. C., and Holben, B. N.:**
25 **Global monitoring of air pollution over land from the Earth Observing System-Terra Moderate**
26 **Resolution Imaging Spectroradiometer (MODIS), *J. Geophys. Res.*, 108(D21), 4661, 2003.**
- 27 Dinar, E., Abo Riziq, A., Spindler, C., Erlick, C., Kiss, G., and Rudich, Y.: The complex refractive
28 index of atmospheric and model humic-like substances (HULIS) retrieved by a cavity ring
29 down aerosol spectrometer (CRD-AS), *Faraday Discuss.*, 137, 279–295, 2008.
- 30 Doherty, S. J., Quinn, P. K., Jefferson, A., Carrico, C. M., Anderson, T. L., and Hegg, D.: A
31 comparison and summary of aerosol optical properties as observed in situ from aircraft, ship,
32 and land during ACE-Asia, *J. Geophys. Res.*, 110, D04201, doi:10.1029/2004jd004964, 2005.
- 33 Eldering, A., Ogren, J. A., Chowdhury, Z., Hughes, L. S., and Cass, G. R.: Aerosol optical properties
34 during INDOEX based on measured aerosol particle size and composition, *J. Geophys. Res.*,
35 107, 8001, doi:10.1029/2001jd001572, 2002.
- 36 Fiedler, S. E., Hese, A., and Ruth, A. A.: Incoherent broad-band cavity-enhanced absorption
37 spectroscopy, *Chem. Phys. Lett.*, 371, 284–294, 2003.
- 38 Garland, R. M., Yang, H., Schmid, O., Rose, D., Nowak, A., Achtert, P., Wiedensohler, A.,
39 Takegawa, N., Kita, K., Miyazaki, Y., Kondo, Y., Hu, M., Shao, M., Zeng, L. M., Zhang, Y. H.,
40 Andreae, M. O., and Pöschl, U.: Aerosol optical properties in a rural environment near the
41 mega-city Guangzhou, China: implications for regional air pollution, radiative forcing and
42 remote sensing, *Atmos. Chem. Phys.*, 8, 5161–5186, doi:10.5194/acp-8-5161-2008, 2008.
- 43 Garland, R. M., Schmid, O., Nowak, A., Achtert, P., Wiedensohler, A., Gunthe, S. S., Takegawa, N.,
44 Kita, K., Kondo, Y., Hu, M., Shao, M., Zeng, L. M., Zhu, T., Andreae, M. O., and Pöschl, U.:

- 1 Aerosol optical properties observed during Campaign of Air Quality Research in Beijing 2006
2 (CAREBeijing-2006): characteristic differences between the inflow and outflow of Beijing city
3 air, *J. Geophys. Res.*, 114, D00g04, doi:10.1029/2008jd010780, 2009.
- 4 Guo, S., Hu, M., Zamora, M. L., Peng, J., Shang, D., Zheng, J., Du, Z., Wu, Z., Shao, M., Zeng, L.,
5 Molina, M. J., and Zhang, R.: Elucidating severe urban haze formation in China, *P. Natl. Acad.*
6 *Sci. USA*, 111, 17373–17378, 2014.
- 7 Han, B., Zhang, R., Yang, W., Bai, Z., Ma, Z., and Zhang, W.: Heavy air pollution episodes in
8 Beijing during January 2013: inorganic ion chemistry and source analysis using Highly Time-
9 Resolved Measurements in an urban site, *Atmos. Chem. Phys. Discuss.*, 15, 11111–11141,
10 doi:10.5194/acpd-15-11111-2015, 2015.
- 11 Han, L., Zhou, W., and Li, W.: Increasing impact of urban fine particles (PM_{2.5}) on areas
12 surrounding Chinese cities, *Scientific Reports*, 5, 12467, doi:10.1038/srep12467, 2015.
- 13 Han, T. T., Liu, X. G., Zhang, Y. H., Qu, Y., Gu, J. W., Ma, Q., Lu, K. D., Tian, H. Z., Chen, J.,
14 Zeng, L. M., Hu, M., and Zhu, T.: Characteristics of aerosol optical properties and their
15 chemical apportionments during CAREBeijing 2006, *Aerosol Air Qual. Res.*, 14, 1431–1442,
16 2014.
- 17 Hand, J. L., and Malm, W. C.: Review of aerosol mass scattering efficiencies from ground-based
18 measurements since 1990, *J. Geophys. Res.*, 112, D16203, doi:10.1029/2007JD008484, 2007.
- 19 Hasan, H. and Dzubay, T. G.: Apportioning light extinction coefficients to chemical species in
20 atmospheric aerosol, *Atmos. Environ.*, 17, 1573–1581, 1983.
- 21 He, X., Li, C. C., Lau, A. K. H., Deng, Z. Z., Mao, J. T., Wang, M. H., and Liu, X. Y.: An intensive
22 study of aerosol optical properties in Beijing urban area, *Atmos. Chem. Phys.*, 9, 8903–8915,
23 doi:10.5194/acp-9-8903-2009, 2009.
- 24 Huang, R. J., Zhang, Y., Bozzetti, C., Ho, K.-F., Cao, J., Han, Y., Dällenbach, K. R., Slowik, J. G.,
25 Platt, S. M., Canonaco, F., Zotter, P., Wolf, R., Pieber, S. M., Bruns, E. A., Crippa, M., Ciarelli,
26 G., Piazzalunga, A., Schwikowski, M., Abbaszade, G., Schnelle-Kreis, J., Zimmermann, R.,
27 An, Z., Szidat, S., Baltensperger, U., Haddad, I. E., and Prévôt, A. S. H.: High secondary
28 aerosol contribution to particulate pollution during haze events in China, *Nature*, 514, 218–222,
29 2014.
- 30 Jung, J., Lee, H., Kim, Y. J., Liu, X. G., Zhang, Y. H., Hu, M., and Sugimoto, N.: Optical properties
31 of atmospheric aerosols obtained by in situ and remote measurements during 2006 Campaign
32 of Air Quality Research in Beijing (CAREBeijing-2006), *J. Geophys. Res.*, 114, D00g02,
33 doi:10.1029/2008jd010337, 2009.
- 34 Lei, Y., Zhang, Q., He, K. B., and Streets, D. G.: Primary anthropogenic aerosol emission trends for
35 China, 1990–2005, *Atmos. Chem. Phys.*, 11, 931–954, doi:10.5194/acp-11-931-2011, 2011.
- 36 Li, C., Marufu, L. T., Dickerson, R. R., Li, Z., Wen, T., Wang, Y., Wang, P., Chen, H., and Stehr,
37 J.W.: In situ measurements of trace gases and aerosol optical properties at a rural site in
38 northern China during East Asian Study of Tropospheric Aerosols: an international regional
39 experiment 2005, *J. Geophys. Res.*, 112, D22S04, doi:10.1029/2006jd007592, 2007.
- 40 Li, L., Chen, J. M., Wang, L., Melluki, W., and Zhou, H. R.: Aerosol single scattering albedo
41 affected by chemical composition: an investigation using CRDS combined with MARGA,
42 *Atmos. Res.*, 124, 149–157, doi:10.1016/j.atmosres.2012.11.007, 2013.
- 43 Lyamani, H., Olmo, F. J., and Alados-Arboledas, L.: Physical and optical properties of aerosols over
44 an urban location in Spain: seasonal and diurnal variability, *Atmos. Chem. Phys.*, 10, 239–254,

1 doi:10.5194/acp-10-239-2010, 2010.

2 Mack, L. A., Levin, E. J. T., Kreidenweis, S. M., Obrist, D., Moosmüller, H., Lewis, K. A., Arnott,
3 W. P., McMeeking, G. R., Sullivan, A. P., Wold, C. E., Hao, W.-M., Collett Jr., J. L., and
4 Malm, W. C.: Optical closure experiments for biomass smoke aerosols, *Atmos. Chem. Phys.*,
5 10, 9017–9026, doi:10.5194/acp-10-9017-2010, 2010.

6 Malm, W. C. and Hand, J. L.: An examination of the physical and optical properties of aerosols
7 collected in the IMPROVE program, *Atmos. Environ.*, 41, 3407–3427,
8 doi:10.1016/j.atmosenv.2006.12.012, 2007.

9 Malm, W. C., Sisler, J. F., Huffman, D., Eldred, R. A., and Cahill, T. A.: Spatial and seasonal trends
10 in particle concentration and optical extinction in the United States, *J. Geophys. Res.*, 99,
11 1347–1370, doi:10.1029/93jd02916, 1994.

12 Marley, N. A., Gaffney, J. S., Castro, T., Salcido, A., and Frederick, J.: Measurements of aerosol
13 absorption and scattering in the Mexico City Metropolitan Area during the MILAGRO field
14 campaign: a comparison of results from the T0 and T1 sites, *Atmos. Chem. Phys.*, 9, 189–206,
15 doi:10.5194/acp-9-189-2009, 2009.

16 Nel, A.: Atmosphere. Air pollution-related illness: effects of particles, *Science*, 308, 804–806, 2005.

17 Peterson, M. R. and Richards, M. H.: Thermal-optical-transmittance analysis for organic, elemental,
18 carbonate, total carbon, and OCX2 in PM_{2.5} by the EPA/NIOSH method, in: *Proceedings,*
19 *Symposium on Air Quality Measurement Methods and Technology-2002*, San Fran- cisco,
20 California, 13–15 November 2002, edited by: Winegar, E. D. and Tropp, R. J., Air and Waste
21 Management Association, Pittsburgh, PA, 83-1–83-19, 2002.

22 Pettersson, A., Lovejoy, E. R., Brock, C. A., Brown, S. S., and Ravishankara, A. R.: Measurement of
23 aerosol optical extinction at with pulsed cavity ring down spectroscopy, *J. Aerosol Sci.*, 35,
24 995–1011, 2004.

25 Pitchford, M., Malm, W., Schichtel, B., Kumar, N., Lowenthal, D., and Hand, J.: Revised algorithm
26 for estimating light extinction from IMPROVE particle speciation data, *J. Air Waste Manage.*,
27 57, 1326–1336, doi:10.3155/1047-3289.57.11.1326, 2007.

28 Quan, J. N., Tie, X., Zhang, Q., Liu, Q., Li, X., Gao, Y., and Zhao, D. L.: Characteristics of heavy
29 aerosol pollution during the 2012–2013 winter in Beijing, China, *Atmos. Environ.*, 88, 83–89,
30 doi:10.1016/j.atmosenv.2014.01.058, 2014.

31 Quinn, P. K.: Aerosol optical properties measured on board the Ronald H. Brown during ACEAsia as
32 a function of aerosol chemical composition and source region, *J. Geophys. Res.- Atmos*, 109,
33 D19S01, doi:10.1029/2003JD004010, 2004.

34 Quinn, P. K., Coffman, D. J., Bates, T. S., Miller, T. L., Johnson, J. E., Voss, K., Welton, E. J., and
35 Neususs, C.: Dominant aerosol chemical components and their contribution to extinction
36 during the aerosols cruise across the Atlantic, *J. Geophys. Res.-Atmos*, 106, 20783–20809,
37 doi:10.1029/2000jd900577, 2001.

38 Quinn, P. K., Coffman, D. J., Bates, T. S., Miller, T. L., Johnson, J. E., Welton, E. J., Neususs, C.,
39 Miller, M., and Sheridan, P. J.: Aerosol optical properties during INDOEX 1999: means,
40 variability, and controlling factors, *J. Geophys. Res.-Atmos*, 107, 8020,
41 doi:10.1029/2000jd000037, 2002.

42 Raes, F., Bates, T., McGovern, F., and Van Liedekerke, M.: The 2nd Aerosol Characterization
43 Experiment (ACE-2): general overview and main results, *Tellus B*, 52, 111–125,
44 doi:10.1034/j.1600-0889.2000.00124.x, 2000. Ramanathan, V., Crutzen, P. J., Kiehl, J. T., and

- 1 Rosenfeld, D.: Aerosols, climate, and the hydrological cycle, *Science*, 294, 2119–2124, 2001.
- 2 Ramanathan, V., Crutzen, P. J., Kiehl, J. T., and Rosenfeld, D.: Aerosols, Climate and the
3 Hydrological Cycle, *Science*, 294, 2119–2124, 2001.
- 4 Ryerson, T. B., Andrews, A. E., Angevine, W. M., Bates, T. S., Brock, C. A., Cairns, B., Cohen, R.
5 C., Cooper, O. R., de Gouw, J. A., Fehsenfeld, F. C., Ferrare, R. A., Fischer, M. L., Flagan, R.
6 C., Goldstein, A. H., Hair, J. W., Hardesty, R. M., Hostetler, C. A., Jimenez, J. L., Langford, A.
7 O., McCauley, E., McKeen, S. A., Molina, L. T., Nenes, A., Oltmans, S. J., Parrish, D. D.,
8 Pederson, J. R., Pierce, R. B., Prather, K., Quinn, P. K., Seinfeld, J. H., Senff, C. J., Sorooshian,
9 A., Stutz, J., Surratt, J. D., Trainer, M., Volkamer, R., Williams, E. J., and Wofsy, S. C.: The
10 2010 California Research at the Nexus of Air Quality and Climate Change (CalNex) field study,
11 *J. Geophys. Res.*, 118, 5830–5866, doi:10.1002/Jgrd.50331, 2013.
- 12 Sun, K., Qu, Y., Wu, Q., Han, T. T., Gu, J. W., Zhao, J. J., Sun, Y. L., Jiang, Q., Gao, Z. Q., Hu, M.,
13 Zhang, Y. H., Lu, K. S. D., Nordmann, S., Cheng, Y. F., Hou, L., Ge, H., Furuuchi, M., Hata,
14 M., and Liu, X. G.: Chemical characteristics of size-resolved aerosols in winter in Beijing, *J.*
15 *Environ. Sci.*, 26, 1641–1650, 2014.
- 16 Sun, Y. L., Wang, Z. F., Fu, P. Q., Yang, T., Jiang, Q., Dong, H. B., Li, J., and Jia, J. J.: Aerosol
17 composition, sources and processes during wintertime in Beijing, China, *Atmos. Chem. Phys.*,
18 13, 4577–4592, doi:10.5194/acp-13-4577-2013, 2013.
- 19 Sun, Y. L., Jiang, Q., Wang, Z. F., Fu, P. Q., Li, J., Yang, T., and Yin, Y.: Investigation of the
20 sources and evolution processes of severe haze pollution in Beijing in January 2013, *J.*
21 *Geophys. Res.-Atmos.*, 119, 4380–4398, doi:10.1002/2014jd021641, 2014.
- 22 Sun, Y. L., Wang, Z. F., Du, W., Zhang, Q., Wang, Q. Q., Fu, P. Q., Pan, X. L., Li, J., Jayne, J., and
23 Worsnop, D. R.: Long-term real-time measurements of aerosol particle composition in Beijing,
24 China: seasonal variations, meteorological effects, and source analysis, *Atmos. Chem. Phys.*
25 *Discuss.*, 15, 14549–14591, doi:10.5194/acpd-15-14549-2015, 2015.
- 26 Takegawa, N., Miyakawa, T., Kuwata, M., Kondo, Y., Zhao, Y., Han, S., Kita, K., Miyazaki, Y.,
27 Deng, Z., Xiao, R., Hu, M., van Pinxteren, D., Herrmann, H., Hofzumahaus, A., Holland, F.,
28 Wahner, A., Blake, D. R., Sugimoto, N., and Zhu, T.: Variability of submicron aerosol
29 observed at a rural site in Beijing in the summer of 2006, *J. Geophys. Res.*, 114, D00g05,
30 doi:10.1029/2008jd010857, 2009.
- 31 Tao, J., Ho, K. F., Chen, L. G., Zhu, L. H., Han, J. L., and Xu, Z. C.: Effect of chemical composition
32 of PM_{2.5} on visibility in Guangzhou, China, 2007 spring, *Partic.*, 7, 68–75,
33 doi:10.1016/j.partic.2008.11.002, 2009.
- 34 Tao, J., Zhang, L., Cao, J., Hsu, S.-C., Xia, X., Zhang, Z., Lin, Z., Cheng, T., and Zhang, R.:
35 Characterization and source apportionment of aerosol light extinction in Chengdu, southwest
36 China, *Atmos. Environ.*, 95, 552–562, doi:10.1016/j.atmosenv.2014.07.017, 2014a.
- 37 Tao, J., Zhang, L., Ho, K., Zhang, R., Lin, Z., Zhang, Z., Lin, M., Cao, J., Liu, S., and Wang, G.:
38 Impact of PM_{2.5} chemical compositions on aerosol light scattering in Guangzhou—the largest
39 megacity in South China, *Atmos. Res.*, 135, 48–58, doi:10.1016/j.atmosres.2013.08.015,
40 2014b.
- 41 Tao, J., Zhang, L. S. M., Gao, J., Wang, H., Chai, F. H., Wang, S. L.: Aerosol chemical composition
42 and light scattering during a winter season in Beijing, *Atmos. Environ.*, 110, 36–44,
43 doi:10.1016/j.atmosenv.2015.03.037, 2015.
- 44 Thompson, J. E., Hayes, P. L., Jimenez, J. L., Adachi, K., Zhang, X., Liu, J., Weber, R. J., and

- 1 Buseck, P. R.: Aerosol optical properties at Pasadena, CA during CalNex 2010, *Atmos.*
2 *Environ.*, 55, 190–200, doi:10.1016/j.atmosenv.2012.03.011, 2012.
- 3 Titos, G., Foyo-Moreno, I., Lyamani, H., Querol, X., Alastuey, A., and Alados-Arboledas, L.:
4 Optical properties and chemical composition of aerosol particles at an urban location: an
5 estimation of the aerosol mass scattering and absorption efficiencies, *J. Geophys. Res.*, 117,
6 D04206, doi:10.1029/2011jd016671, 2012.
- 7 Turpin, B. J. and Lim, H. J.: Species contributions to PM_{2.5} mass concentrations: revisiting common
8 assumptions for estimating organic mass, *Aerosol Sci. Tech.*, 35, 602–610,
9 doi:10.1080/02786820119445, 2001.
- 10 Varma, R., Moosmüller, H., and Arnott, W. P.: Toward an ideal integrating nephelometer, *Opt. Lett.*,
11 28, 1007–1009, 2003.
- 12 Wang, L., Li, Z., Tian, Q., Ma, Y., Zhang, F., Zhang, Y., Li, D., Li, K., and Li L.: Estimate of
13 aerosol absorbing components of black carbon, brown carbon, and dust from ground-based
14 remote sensing data of sun-sky radiometers, *J. Geophys. Res. Atmos.*, 118, 6534–6543,
15 doi:10.1002/jgrd.50356, 2013.
- 16 Wang, X., Huang, J., Zhang, R., Chen, B., and Bi, J.: Surface measurements of aerosol properties
17 over northwest China during ARM China 2008 deployment, *J. Geophys. Res.*, 115, D00K27,
18 doi:10.1029/2009JD013467, 2010.
- 19 Wang, X. F., Wang, T., Pathak, R. K., Hallquist, M., Gao, X. M., Nie, W., Xue, L. K., Gao, J., Gao,
20 R., Zhang, Q. Z., Wang, W. X., Wang, S. L., Chai, F. H., and Chen, Y. Z.: Size distributions of
21 aerosol sulfates and nitrates in Beijing during the 2008 Olympic Games: impacts of pollution
22 control measures and regional transport, *Adv. Atmos. Sci.*, 30, 341–353, 2013.
- 23 Wang, Y. H., Liu, Z. R., Zhang, J. K., Hu, B., Ji, D. S., Yu, Y. C., and Wang, Y. S.: Aerosol
24 physicochemical properties and implications for visibility during an intense haze episode
25 during winter in Beijing, *Atmos. Chem. Phys.*, 15, 3205–3215, doi:10.5194/acp-15-3205-2015,
26 2015.
- 27 Watson, J. G.: Visibility: science and regulation, *J. Air Waste Manage.*, 52, 628–713, 2002.
- 28 Wu, Q. Z., Wang, Z. F., Gbaguidi, A., Gao, C., Li, L. N., and Wang, W.: A numerical study of
29 contributions to air pollution in Beijing during CAREBeijing-2006, *Atmos. Chem. Phys.*, 11,
30 5997–6011, doi:10.5194/acp-11-5997-2011, 2011.
- 31 Wu, Z. J., Zheng, J., Shang, D. J., Du, Z. F., Wu, Y. S., Zeng, L. M., Wiedensohler, A., and Hu, M.:
32 Particle hygroscopicity and its link to chemical composition in the urban atmosphere of Beijing,
33 China during summertime, *Atmos. Chem. Phys. Discuss.*, 15, 11495–11524,
34 doi:10.5194/acpd-15-11495-2015, 2015.
- 35 Xu, J., Ma, J. Z., Zhang, X. L., Xu, X. B., Xu, X. F., Lin, W. L., Wang, Y., Meng, W., and Ma, Z. Q.:
36 Measurements of ozone and its precursors in Beijing during summertime: impact of urban
37 plumes on ozone pollution in downwind rural areas, *Atmos. Chem. Phys.*, 11, 12241–12252,
38 doi:10.5194/acp-11-12241-2011, 2011.
- 39 Xu, X., Zhao, W., Wang, S., Zhang, Q., Qian, X., Fang, B., Venables, D. S., Chen, W., Gao, X., and
40 Zhang, W.: Retrieval of the particulate complex refractive index by using cavity enhanced
41 aerosol albedometer, in preparation, 2016.
- 42 Yan, P., Tang, J., Huang, J., Mao, J. T., Zhou, X. J., Liu, Q., Wang, Z. F., and Zhou, H. G.: The
43 measurement of aerosol optical properties at a rural site in Northern China, *Atmos. Chem.*
44 *Phys.*, 8, 2229–2242, doi:10.5194/acp-8-2229-2008, 2008.

- 1 Yang, L. X., Wang, D. C., Cheng, S. H., Wang, Z., Zhou, Y., Zhou, X. H., and Wang, W. X.:
2 Influence of meteorological conditions and particulate matter on visual range impairment in
3 Jinan, China, *Sci. Total Environ.*, 383, 164–173, doi:10.1016/j.scitotenv.2007.04.042, 2007.
- 4 Yang, Y. R., Liu, X. G., Qu, Y., An, J. L., Jiang, R., Zhang, Y. H., Sun, Y. L., Wu, Z. J., Zhang, F.,
5 Xu, W. Q., and Ma, Q. X.: Characteristics and formation mechanism of continuous hazes in
6 China: a case study during the autumn of 2014 in the North China Plain, *Atmos. Chem. Phys.*,
7 15, 8165–8178, doi:10.5194/acp-15-8165-2015, 2015.
- 8 Yao, T., Huang, X., He, L., Hu, M., Sun, T., Xue, L., Lin, Y., Zeng, L., and Zhang, Y.: High time
9 resolution observation and statistical analysis of atmospheric light extinction properties and the
10 chemical speciation of fine particulates, *Sci. China Chem.*, 53, 1801–1808,
11 doi:10.1007/s11426-010-4006-z, 2010.
- 12 Zhang, A., Qi, Q. W., Jiang, L. L., Zhou, F., and Wang, J. F.: Population exposure to PM_{2.5} in the
13 urban area of Beijing, *PLoS One*, 8, e63486, 2013.
- 14 Zhang, H., Hu, D., Chen, J., Ye, X., Wang, X., Hao, J., Wang, L., Zhang, R., and An, Z.: Particle
15 size distribution and polycyclic aromatic hydrocarbons emissions from agricultural crop
16 residue burning, *Environ. Sci. Technol.*, 45, 5477–5482, 2011.
- 17 Zhang, X., Lin, Y. H., Surratt, J. D., and Weber, R. J.: Sources, composition and absorption
18 Angstrom exponent of light-absorbing organic components in aerosol extracts from the Los
19 Angeles Basin, *Environ. Sci. Technol.*, 47, 3685–3693, doi:10.1021/es305047b, 2013.
- 20 Zhang, Y. H., Hu, M., Zhong, L. J., Wiedensohler, A., Liu, S. C., Andreae, M. O., Wang, W., and
21 Fan, S. J.: Regional Integrated Experiments on Air Quality over Pearl River Delta 2004
22 (PRIDE-PRD2004): overview, *Atmos. Environ.*, 42, 6157–6173,
23 doi:10.1016/j.atmosenv.2008.03.025, 2008.
- 24 Zhao, W., Dong, M., Chen, W., Gu, X., Hu, C., Gao, X., Huang, W., and Zhang, W.:
25 Wavelength-resolved optical extinction measurements of aerosols using broad-band
26 cavity-enhanced absorption spectroscopy over the spectral range of 445–480 nm, *Anal. Chem.*,
27 85, 2260–2268, doi:10.1021/ac303174n, 2013.
- 28 Zhao, W., Xu, X., Dong, M., Chen, W., Gu, X., Hu, C., Huang, Y., Gao, X., Huang, W., and Zhang,
29 W.: Development of a cavity-enhanced aerosol albedometer, *Atmos. Meas. Tech.*, 7,
30 2551–2566, doi:10.5194/amt-7-2551-2014, 2014a.
- 31 Zhao, W., Xu, X., Dong, M., Chen, W., Gao, X., Huang, W., and Zhang, W.: Development of a
32 cavity-enhanced albedometer for simultaneous measurement of aerosol extinction and
33 scattering coefficients, in *imaging and applied optics 2014*, OSA Technical Digest (online)
34 (Optical Society of America), paper JTU4A.43, 2014b.
- 35 Zhao, X. J., Zhao, P. S., Xu, J., Meng, W., Pu, W. W., Dong, F., He, D., and Shi, Q. F.: Analysis of a
36 winter regional haze event and its formation mechanism in the North China Plain, *Atmos.*
37 *Chem. Phys.*, 13, 5685–5696, doi:10.5194/acp-13-5685-2013, 2013.
- 38 Zheng, G. J., Duan, F. K., Su, H., Ma, Y. L., Cheng, Y., Zheng, B., Zhang, Q., Huang, T., Kimoto, T.,
39 Chang, D., Pöschl, U., Cheng, Y. F., and He, K. B.: Exploring the severe winter haze in Beijing:
40 the impact of synoptic weather, regional transport and heterogeneous reactions, *Atmos. Chem.*
41 *Phys.*, 15, 2969–2983, doi:10.5194/acp-15-2969-2015, 2015.
- 42 Zheng, S., Pozzer, A., Cao, C. X., and Lelieveld, J.: Long-term (2001–2012) concentrations of fine
43 particulate matter (PM_{2.5}) and the impact on human health in Beijing, China, *Atmos. Chem.*
44 *Phys.*, 15, 5715–5725, doi:10.5194/acp-15-5715-2015, 2015.

1 Zhou, X. H., Gao, J., Wang, T., Wu, W. S., and Wang, W. X.: Measurement of black carbon aerosols
2 near two Chinese megacities and the implications for improving emission inventories, *Atmos.*
3 *Environ.*, 43, 3918–3924, doi:10.1016/j.atmosenv.2009.03.062, 2009.

4

5

6

7

1
2
3
4
5
6
7
8
9

Table 1. List of the mean optical values (aerosol extinction, scattering, absorption coefficients, and SSA at $\lambda = 470$ nm), the effective mode diameters (particle number, surface area and volume, fitted values from the measured submicron size distribution with mono-lognormal distribution function), and chemical composition of PM_{1.0} particles observed in this campaign. These parameters were classified into three different pollution levels (clear, slightly polluted and polluted days).

Parameter	Clear	Slightly Polluted	Polluted	All days	
Optical	$\alpha_{ep,470}$ (Mm ⁻¹)	58.6±81.6	186.7±161.6	567.9±292.3	200.9±239.6
	$\alpha_{sp,470}$ (Mm ⁻¹)	47.2±64.7	148.9±131.9	477.2±255.5	163.9±201.7
	$\alpha_{ap,470}$ (Mm ⁻¹)	11.6±18.3	37.8±32.3	90.9±55.8	37.0±43.2
	ω_{470}	0.81±0.10	0.79±0.07	0.84±0.06	0.80±0.08
Size	$D_{p,n}$ (nm)	38±31	73±51	120±64	67±55
	$D_{p,s}$ (nm)	374±130	338±114	335±76	351±116
	$D_{p,v}$ (nm)	478±94	480±90	455±82	475±91
Chemical Composition ($\mu\text{g}/\text{m}^3$)	OC	3.41±2.43	8.81±4.64	20.47±6.93	8.34±6.97
	EC	0.48±0.39	1.18±0.59	2.72±0.87	1.12±0.92
	NO ₃ ⁻	1.78±1.70	5.12±3.56	14.99±6.54	5.19±5.52
	SO ₄ ²⁻	1.29±0.69	3.20±2.25	9.62±4.55	3.35±3.52
	NH ₄ ⁺	0.72±0.75	2.98±2.32	9.31±4.33	2.98±3.57
	Cl ⁻	0.52±0.96	1.48±1.41	4.46±2.26	1.52±1.88
	Ca ²⁺	0.31±0.27	0.62±0.38	0.58±0.33	0.49±0.36
	K ⁺	0.16±0.25	0.50±0.38	1.18±0.46	0.46±0.48
	Na ⁺	0.19±0.22	0.33±0.28	0.60±0.38	0.32±0.30
	Mg ²⁺	0.04±0.03	0.08±0.03	0.09±0.03	0.06±0.04

10

11 Table 2. List of aerosol mean diameters and optical properties during the selected haze episode.

12

13

14

Episode	Date (LT)	Number mean diameter (nm)	Surface mean diameter (nm)	$\alpha_{ep,470}$ (Mm^{-1})	$\alpha_{sp,470}$ (Mm^{-1})	$\alpha_{ap,470}$ (Mm^{-1})	ω_{470}	Real part of effective CRI (n)	Imaginary part of effective CRI (k)
Period 1	22 Nov 05:40–10:00	56±6	193±19	56±24	44±19	12±6	0.79±0.03	1.38±0.06	0.03±0.02
Period 2	22 Nov 12:40–15:00	25±4	193±17	17±5	16±5	1.0±0.4	0.94±0.03	1.40±0.06	0.008±0.005
Period 3	22 Nov 15:30–23 Nov 08:00	106±16	229±16	179±69	151±57	28±12	0.85±0.01	1.39±0.04	0.02±0.006
Period 4	23 Nov 08:30–12:00	105±16	251±15	405±60	321±42	84±22	0.79±0.03	1.40±0.03	0.034±0.008
Period 5	23 Nov 12:30–24 Nov 07:30	124±19	263±11	330±110	283±94	46±16	0.86±0.01	1.44±0.03	0.02±0.01
Period 6	24 Nov 08:00–11:10	80±42	226±14	80±42	64±34	16±8	0.78±0.04	1.40±0.04	0.04±0.02

15

16

17

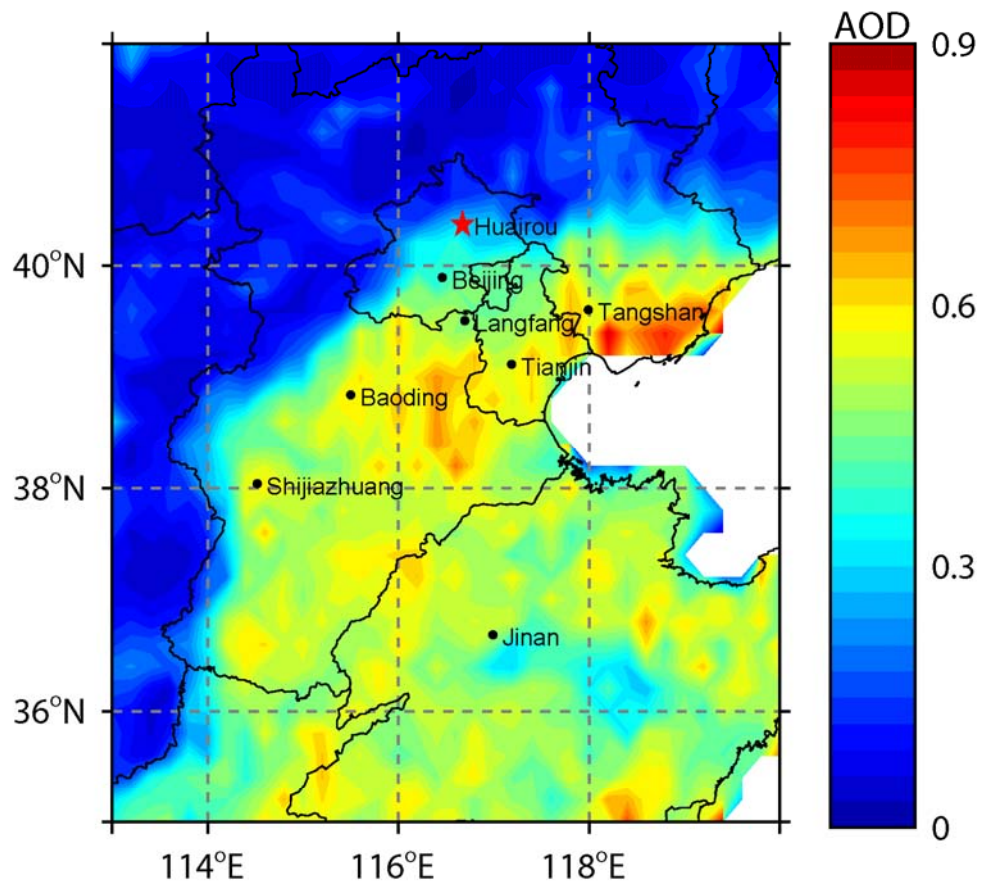
18 Table 3. List of the mean values of aerosol scattering, absorption coefficients, and single scattering albedo in this campaign and recently reported
 19 values from references.

20

Location	Date (MM/yy)	λ (nm)	α_{sp} (Mm^{-1})	α_{ap} (Mm^{-1})	ω_0	RH	Inlet	References
Granada, Spain (Urban)	03/2006 - 02/2007	α_{sp} : 550 α_{ap} : 550	61±25	24±9	0.71±0.07	<50%	PM ₁₀	Titos et al.(2012)
Guangzhou (Urban)	07/2006	α_{sp} : 550 α_{ap} : 532	151±103	34±27	0.82±0.07	<40%	PM ₁₀	Garland et al.(2008)
Beijing (Urban)	01/2005 - 12/2006	α_{sp} : 525 α_{ap} : 532	255±243	45±39	0.80±0.09	<60%	TSP	He et al.(2009)
Shanghai (Urban)	04 - 05/2010	α_{sp} : 532 α_{ap} : 532	102±74	44±35	0.70±0.07	41.2%	TSP	Li et al.(2013)
Xinken, (Suburban)	PRD 10/2004 - 11/2004	α_{sp} : 550 α_{ap} : 630	333±138	70±42	0.83±0.05	<20%	PM ₁₀	Cheng et al.(2008)
Xianghe, (Suburban)	Beijing 03/2005	α_{sp} : 550 α_{ap} : 550	468±472	65±75	0.81-0.85	<42.5%	TSP	Li et al.(2007)
Yufa, (Suburban)	Beijing 08/2006 - 09/2006	α_{sp} : 550 α_{ap} : 532	361±295	52±37	0.86±0.07	<32%	PM ₁₀	Garland et al.(2009)
Huairou, (Suburban)	Beijing 11/2014 - 01/2015	α_{sp} : 470 α_{ap} : 470	164±202	37±43	0.80±0.08	<15%	PM_{1.0}	This work
Shangdianzi, Beijing (Rural)	09/2003 - 01/2005	α_{sp} : 525 α_{ap} : 525	175±189	18±13	0.88±0.05	<60%	TSP	Yan et al.(2008)
Pasadena, US (Rural)	05/2010 - 06/2010	α_{sp} : 532 α_{ap} : 532	58±43	4±4	0.92±0.08	<50%	PM _{1.0}	Thompson et al.(2012)

21

22

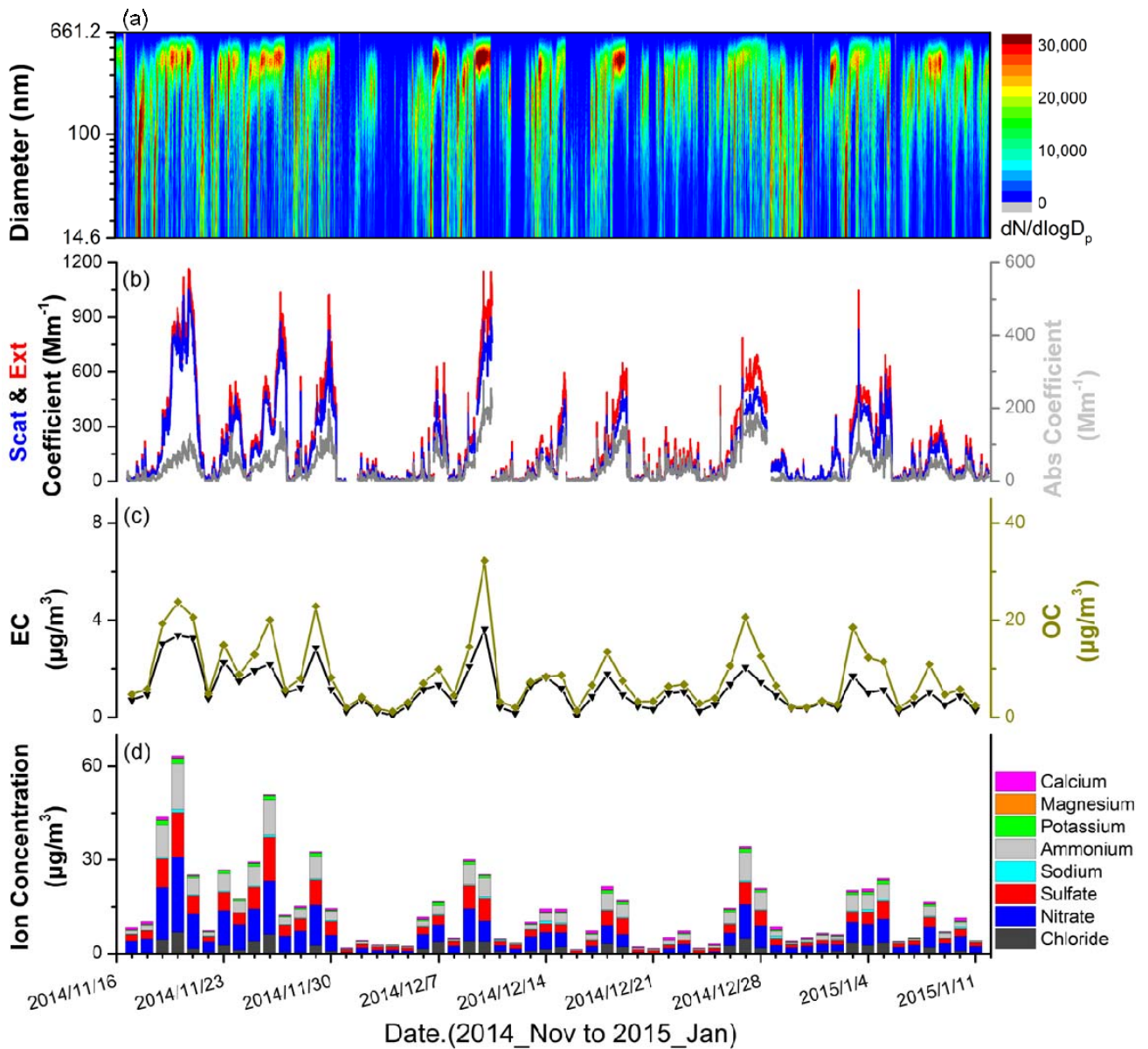


23
 24
 25
 26
 27
 28
 29
 30

Fig. 1. The map of the North China Plain. The observation site (Huairou) is marked with red star. The contour plot represents the average distribution of the MODIS AOD with $0.2^{\circ} \times 0.2^{\circ}$ resolution during the campaign (16 November 2014 to 11 January 2015).

31

32



33

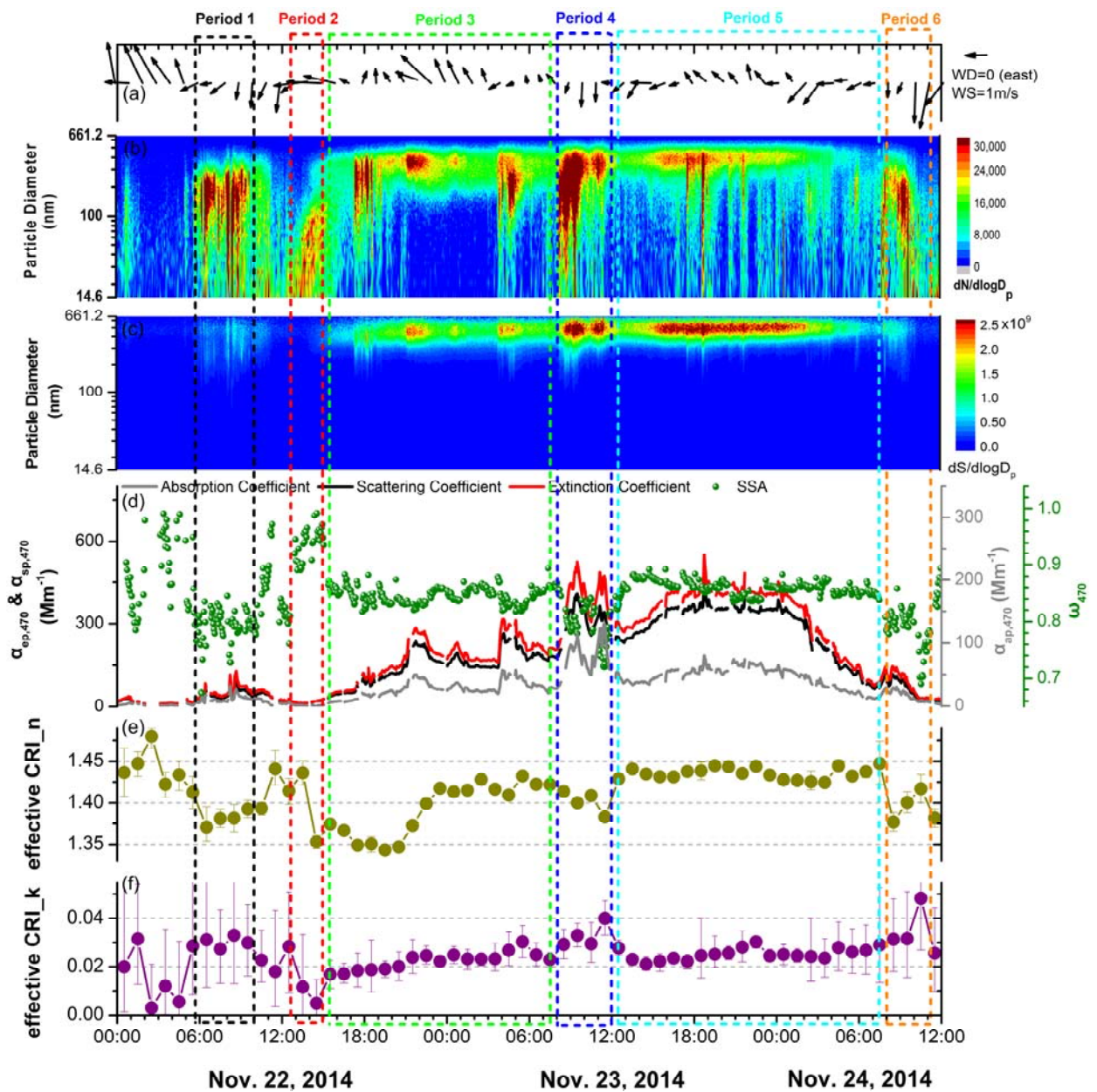
34

35

36 Fig. 2. Time series of (a) the aerosol number size distribution measured by SMPS, (b) the extinction,
 37 scattering and absorption coefficients at $\lambda = 470$ nm measured by cavity enhanced albedometer, (c)
 38 organic carbon and element carbon concentration measured with an off-line aerosol carbon analyzer,
 39 and (d) water-insoluble ion concentrations measured with an off-line ion chromatography of dry
 40 $PM_{1.0}$ particles over the sampling period.

41

42



44

45

46

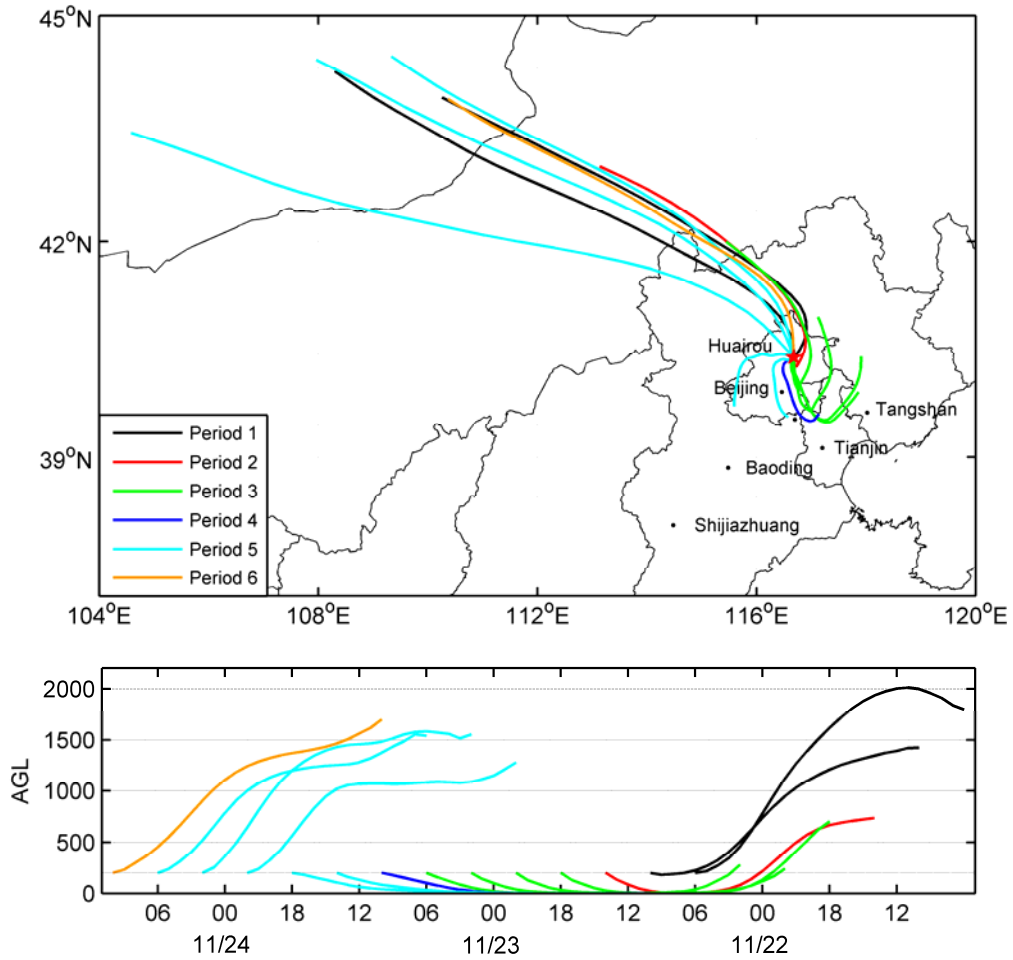
47

48 Fig. 3 Highly time-resolved evolution of a selected air pollution episode during November 22 to 24,
 49 2014. (a) particle number size distribution, (b) particle surface size distribution, (c) aerosol extinction,
 50 scattering, absorption coefficients, and SSA at $\lambda = 470$ nm, (d) retrieved real part of CRI, (e)
 51 retrieved imaginary part of CRI. The air pollution episode was divided into six shorter periods to
 52 clearly show the evaluation of optical properties during haze formation, development and decline.

53

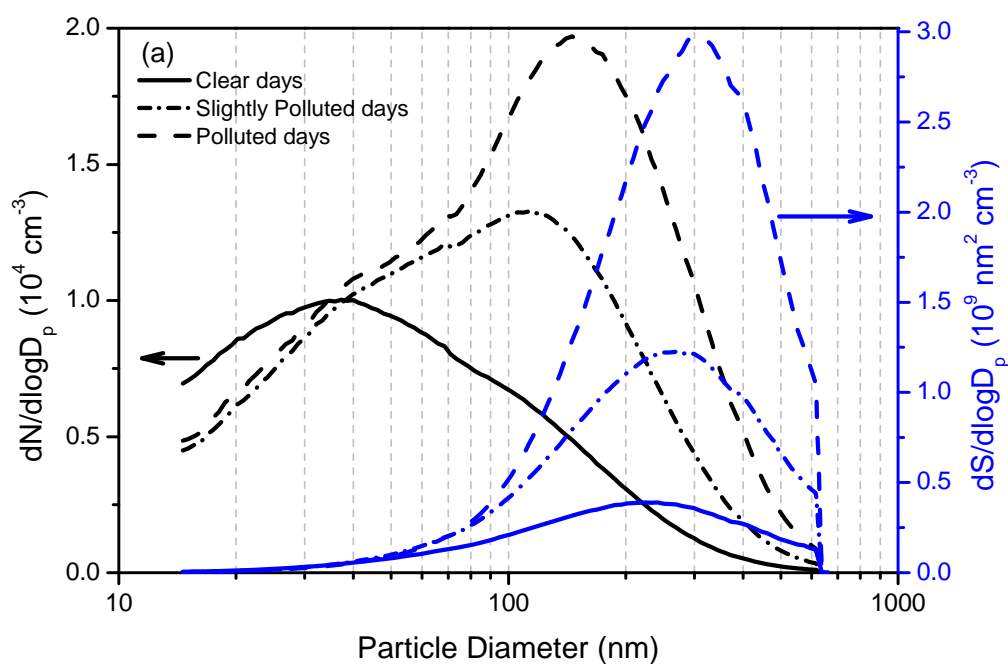
54

55
56
57
58

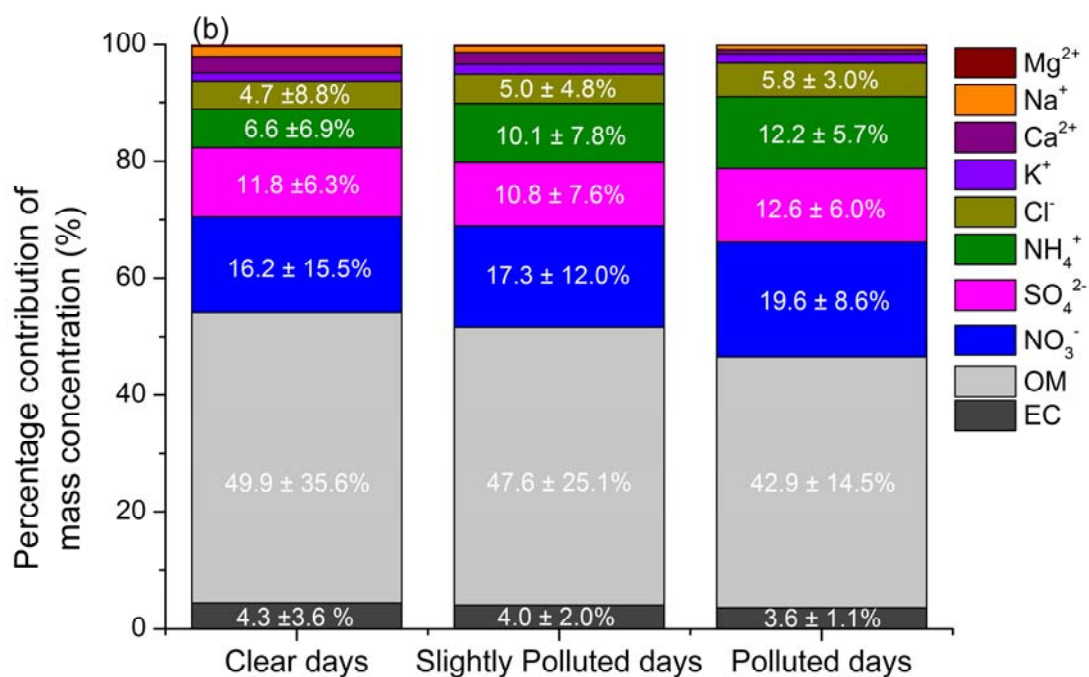


59
60
61
62
63
64
65
66
67
68

Fig. 4 The 24 hour back trajectories starting at 200 m above ground level in Huairou site were calculated every 4 h (at 00:00, 06:00, 12:00 and 18:00 local time) during the selected air pollution episode.



69



70

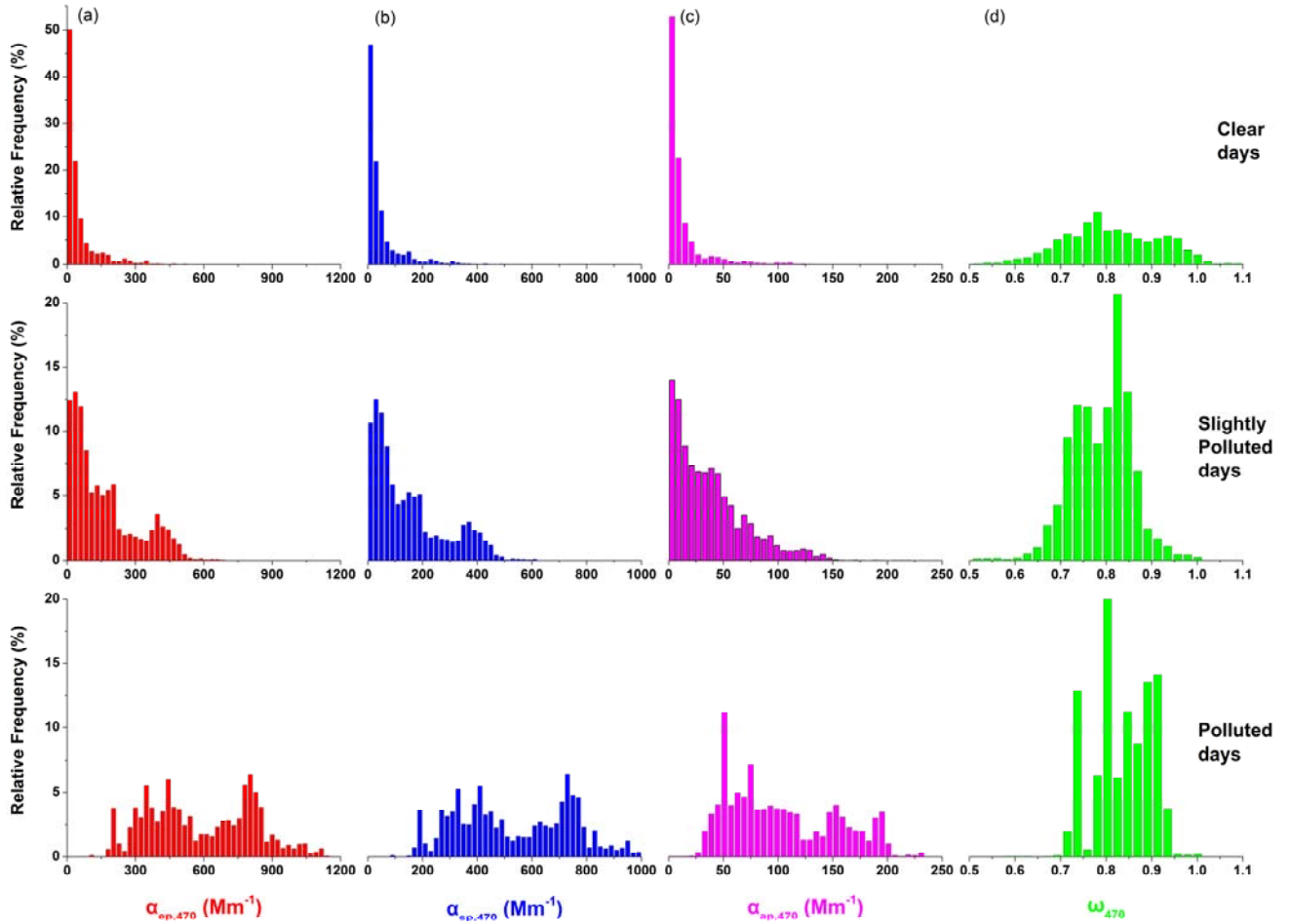
71

72 Fig. 5 (a) The mean number and surface size distribution and (b) percentage contribution of the mass
 73 concentrations of OM, EC concentrations and eight water-soluble ion components on clear, slightly
 74 polluted and polluted days.

75

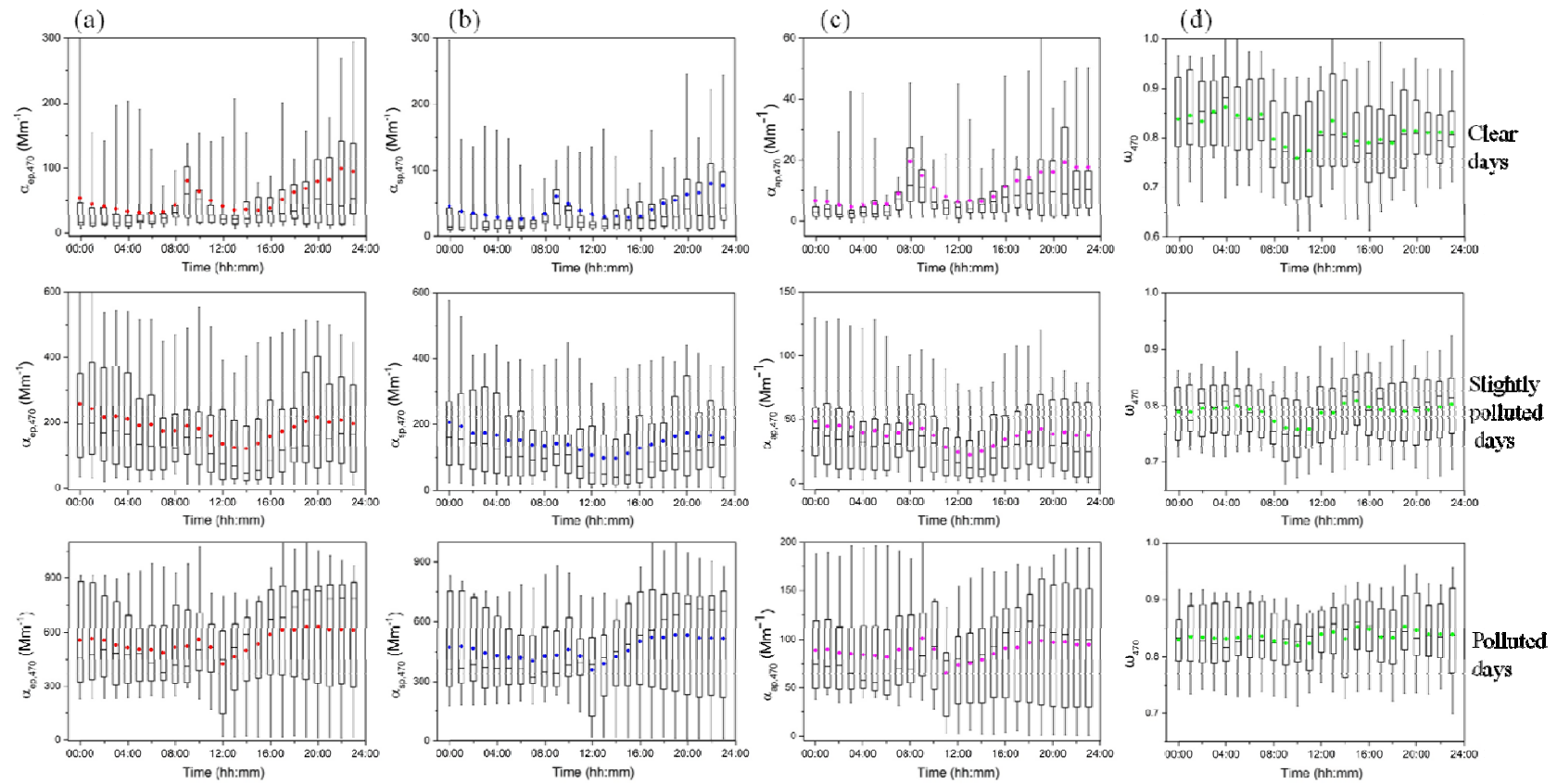
76

77
78
79



80
81
82
83
84
85
86
87
88

Fig 6. The frequency distributions of dry $PM_{1.0}$ optical properties at $\lambda = 470$ nm observed during the campaign. (a) extinction coefficient, (b) scattering coefficient, (c) absorption coefficient, (d) single scattering albedo on clear, slightly polluted and polluted days.



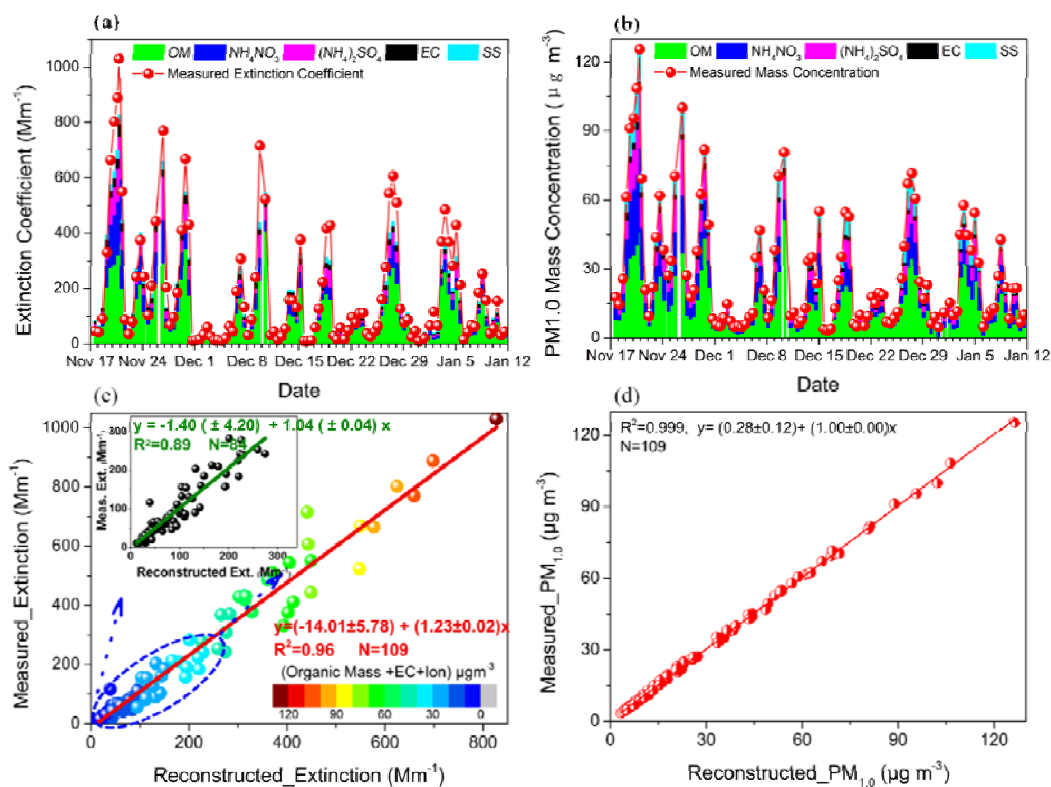
90

91

92 Fig. 7 Diurnal variations of hourly averaged (a) extinction coefficient, (b) scattering coefficient, (c) absorption coefficient and (d) SSA at $\lambda = 470$
 93 nm on clear, slightly polluted and polluted days. The error bars are 5th and 95th percentiles and the limits of the boxes represent 25th and 75th
 94 percentiles.

95

96
97
98
99
100



101
102
103
104
105
106
107
108
109
110
111
112
113

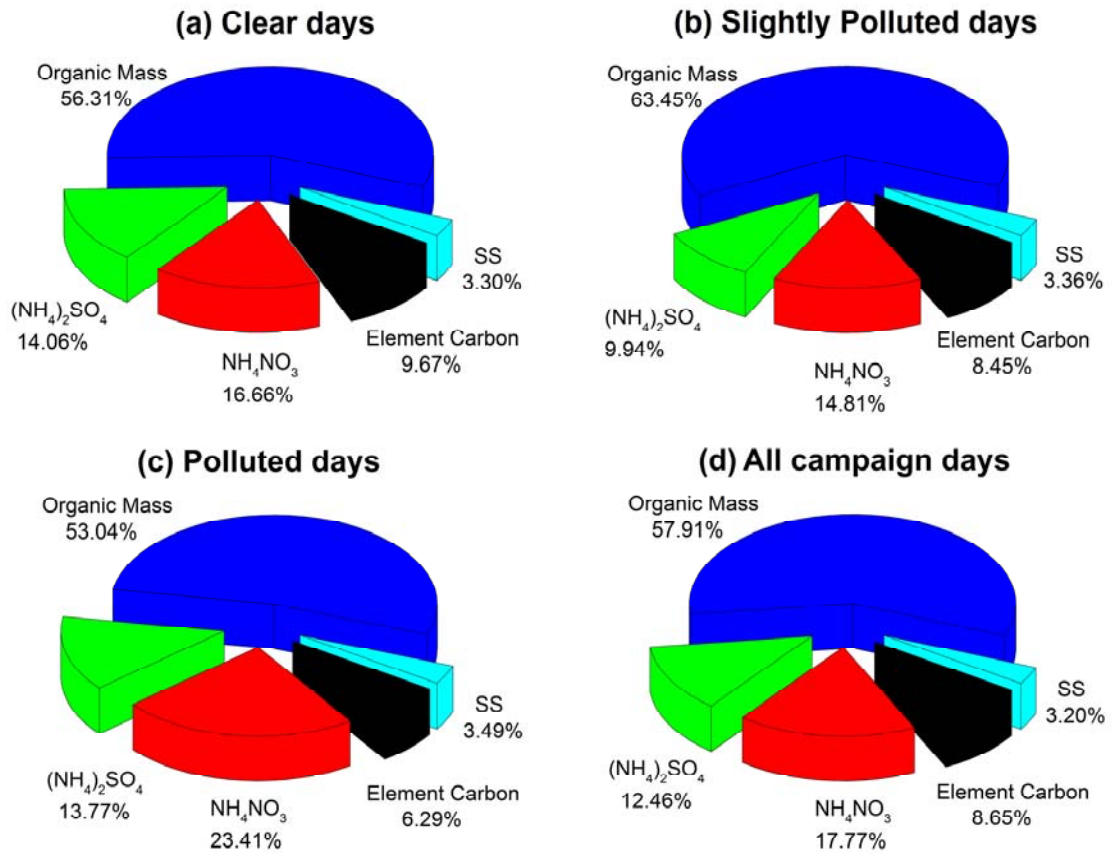
Fig. 8 (a) and (b) : The plot of measured and reconstruction value of the extinction and mass concentration, respectively; (c) and (d) : Scatter plot of the measured extinction coefficient at $\lambda = 470$ nm and $PM_{1.0}$ mass concentration against the reconstructed values with the modified IMPROVE formula. Insert of (c) shows the linear regression between measured and reconstructed extinction coefficient under lower aerosol load condition (with extinction smaller than $300 Mm^{-1}$).

114

115

116

117



118

119

120

121

122

123

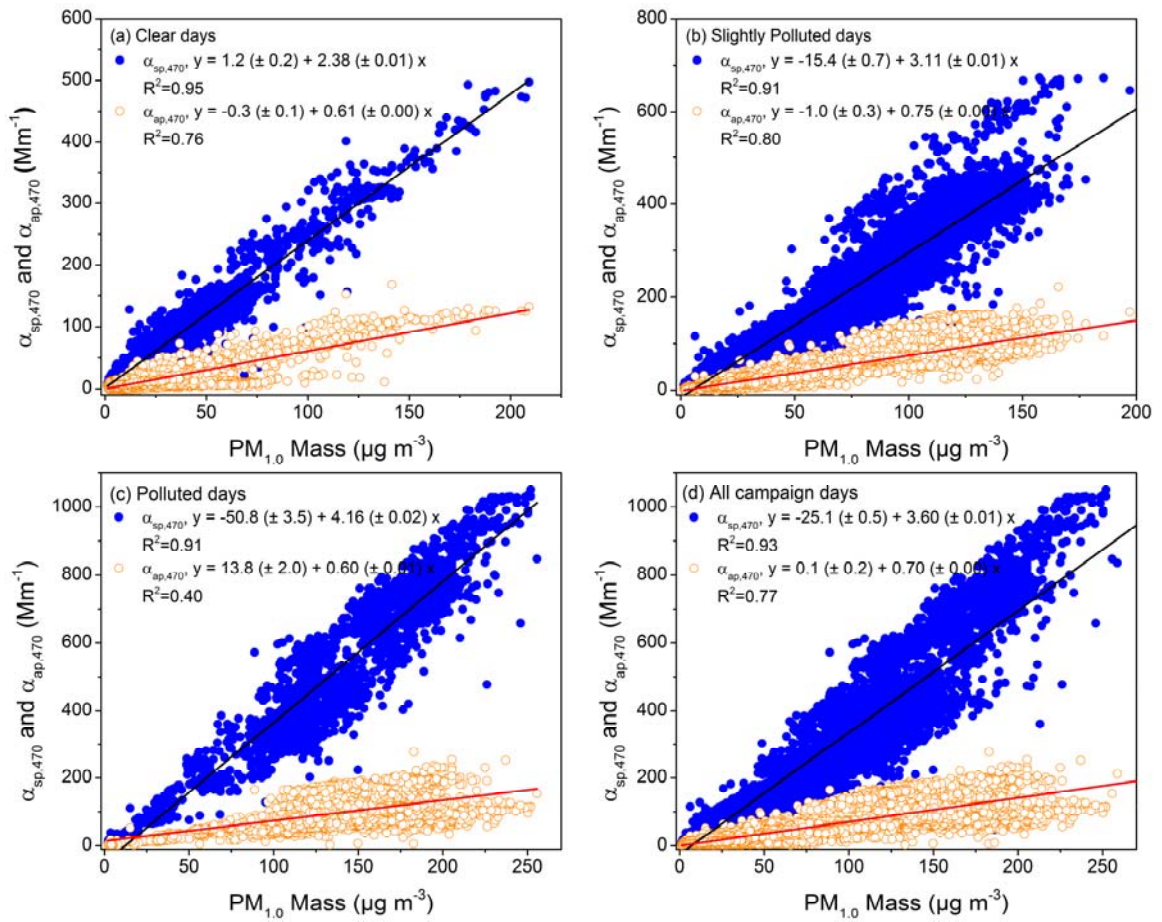
124

125 Fig. 9 Average fractional contribution of each chemical composition to dry $\text{PM}_{1.0}$
126 extinction coefficient with respect to different pollution level.

127

128

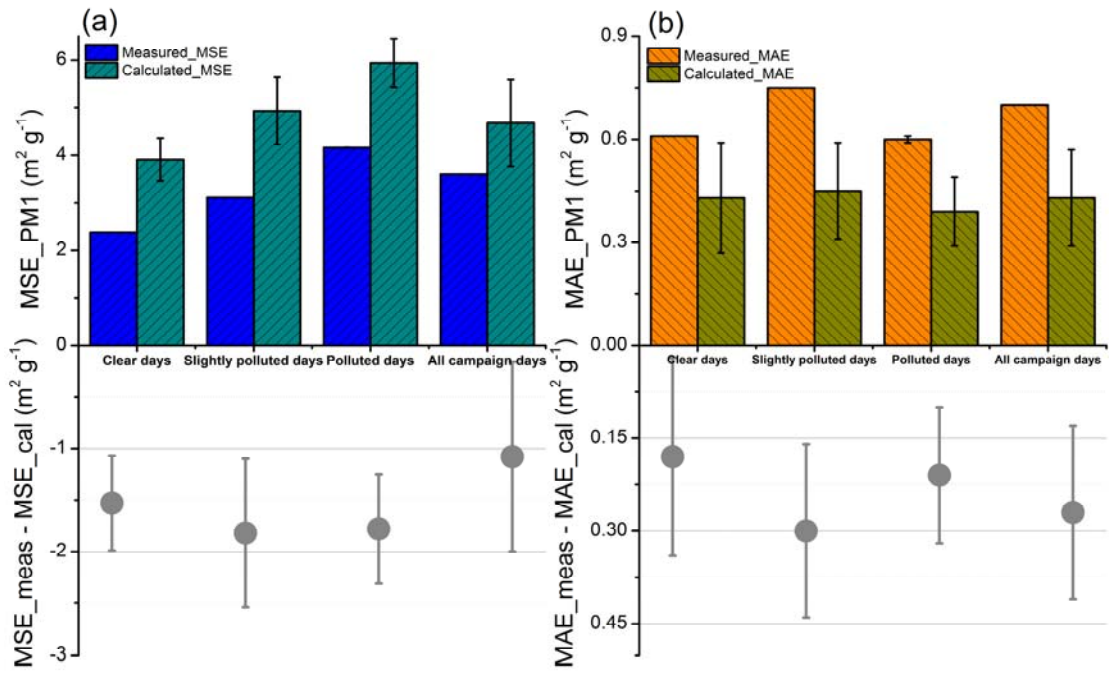
129
130
131
132
133



134
135
136
137
138
139
140
141
142
143

Fig. 10 Scatter plots of the measured scattering and absorption coefficients at $\lambda = 470$ nm against $PM_{1.0}$ mass concentrations for $PM_{1.0}$ particles under different pollution level.

144
145
146
147
148
149



150
151
152
153
154
155
156
157
158 Fig. 11 Comparisons of measured and reconstructed (a) MSE and (b) MAE of $\text{PM}_{1.0}$
159 particles under different pollution level.
160